2. EXPLANATORY NOTES[1]

Shipboard Scientific Party[2]

INTRODUCTION

In this chapter, we have assembled information that will help the reader understand the basis for our preliminary conclusions and also help the interested investigator select samples for further analysis. This information concerns only shipboard operations and analyses described in the site reports in the *Initial Reports* volume of the Leg 127 *Proceedings of the Ocean Drilling Program*. Methods used by various investigators for shore-based analysis of Leg 127 data will be detailed in the individual scientific contributions published in the *Scientific Results* volume.

AUTHORSHIP OF SITE CHAPTERS

The separate sections of the site chapters were written by the following shipboard scientists (authors are listed in alphabetical order in parentheses, no seniority is necessarily implied):

Site Summary (Pisciotto, Tamaki)
Background and Objectives (Pisciotto, Tamaki)
Operations (Foss, Pisciotto, Tamaki)
Lithostratigraphy (Barnes, Boggs, Cramp, Jolivet, Mertz, Tada)
Biostratigraphy (Alexandrovich, Brunner, Koizumi, Rahman, White)
Paleomagnetics (Vigliotti, Wippern)
Sediment Accumulation Rates (Alexandrovich, Brunner, Koizumi, Rahman, White)
Inorganic Geochemistry (Brumsack, Murray)
Organic Geochemistry (Kawka, McEvoy)
Basement Rocks (Allan, Stewart, Thy, Yamashita)
Physical Properties (Kuramoto, Langseth, Nobes)
Downhole Measurements (Langseth, Meredeth, Schaar)
Conclusions (Pisciotto, Tamaki)
Appendix (Shipboard Party)

Summary core descriptions ("barrel sheets" and igneous rock visual core descriptions) and photographs of each core appear at the end of the volume.

DEFINITIONS

Conventional Use of Time and Time-Rock Units

The subdivisions of epochs/series into early, middle, late, or lower, middle, upper have no real formal standing in stratigraphy. The subdivision of lithostratigraphic (rock), chronostratigraphic (time-rock), and geochronologic (time) units is defined as follows throughout this volume.

1. Lithostratigraphic units: For rock units, the terms lower, middle, and upper describe sections of rocks subdivided on the basis of superposition, without any implication of time-partitioning.

2. Chronostratigraphic units: These units imply bodies of strata formed during specific intervals of geologic time. According to convention they are subdivided using the terms lower, middle, and upper. The basis of formal time-rock units are stages, each of which has (or should have) a stratotype, a standard section with which other sections can be compared. Stages are conventionally grouped together into the subunits that subdivide the series. When referring to the entire subdivision of the series, we capitalized the terms Lower, Middle, and Upper. The lowercase forms, lower, middle, and upper, refer only to a portion of the subunit or its equivalent, or instead imply informal usage.

3. Geochronologic units: When speaking of time, age, or of sections in the temporal sense, the terms early, middle, and late are used for subdivision. The basis of the formal geochronologic units are ages (time equivalent of stages). Like stages, ages grouped together form the time subunits that subdivide epochs. When we refer to the entire subunit, the terms Early, Middle, Late are capitalized, but not when only a part of the subunit, or an informal sense is implied. However, such combinations as early Early, middle Early, late Early, etc., are used to refer to older, medial, or younger parts of the entire subunit.

Use of Ma vs. m.y.

1. The expression Ma is equivalent to and replaces m.y.B.P. (million years Before Present), e.g., 35–40 Ma.

2. The expression m.y. is used in sentences such as, "for five m.y. in the early Miocene."

DRILLING CHARACTERISTICS

Information concerning sedimentary stratification in uncored or unrecovered intervals may be inferred from seismic data, wireline-logging results, and from an examination of the behavior of the drill string as observed and recorded on the drilling platform. Typically, the harder a layer, the slower and more difficult it is to penetrate. A number of other factors may determine the rate of penetration, so it is not always possible to relate the drilling time directly to the hardness of the layers. Bit weight and revolutions per minute, recorded on the drilling recorder, also influence the penetration rate.

DRILLING DEFORMATION

When cores are split, many show signs of significant sediment disturbance, including the concave-downward appearance of originally horizontal bands, haphazard mixing of lumps of different lithologies (mainly at the tops of cores), and the near-fluid state of some sediments recovered from tens to hundreds of meters below the seafloor. Core deformation probably occurs during cutting, retrieval (with accompanying changes in pressure and temperature), and core handling on deck.

---

[1] Tamaki, K., Pisciotto, K., Allan, J., et al., 1990. *Proc. ODP, Init. Repts.*, 127: College Station, TX (Ocean Drilling Program).

[2] Shipboard Scientific Party is as given in the list of participants preceding the contents.

SHIPBOARD SCIENTIFIC PROCEDURES

Numbering of Sites, Holes, Cores, and Samples

ODP drill sites are numbered consecutively, and refer to one or more holes drilled while the ship was positioned over one acoustic beacon. Multiple holes may be drilled at a single site by pulling the drill pipe above the seafloor (out of the hole), moving the ship some distance from the previous hole, and then drilling another hole.

For all ODP drill sites, a letter suffix distinguishes each hole drilled at the same site. For example, the first hole drilled is assigned the site number modified by the suffix A, the second hole takes the site number and suffix B, and so forth. Note that this procedure differs slightly from that used by DSDP (Sites 1 through 624), but prevents ambiguity between site- and hole-number designations. It is important to distinguish among holes drilled at a site, because recovered sediments or rocks from different holes usually do not come from equivalent positions in the stratigraphic column.

The cored interval is measured in meters below seafloor (mbsf). The depth interval assigned to an individual core begins with the depth below the seafloor that the coring operation began, and extends to the depth that the coring operation ended (see Fig. 1). For example, each coring interval is generally up to 9.5 m long, which is the capacity of a core barrel. Coring intervals may be shorter and may not necessarily be adjacent if separated by drilled intervals. In soft sediments, the drill string can be "washed ahead" with the core barrel in place, without recovering sediments. This is achieved by pumping water down the pipe at high pressure to wash the sediment out of the way of the bit and up the space between the drill pipe and the wall of the hole. If thin, hard, rock layers are present, then it is possible to get "spotty" sampling of these resistant layers within the washed interval, and thus to have a cored interval greater than 9.5 m. In drilling hard rock, a center bit may replace the core barrel if necessary to drill without core recovery.

Cores taken from a hole are numbered serially from the top of the hole downward. Core numbers and their associated cored intervals in meters below seafloor usually are unique in a given hole; however, this may not be true if an interval must be cored twice, because of caving of cuttings or other hole problems. Maximum full recovery for a single core is 9.5 m of rock or sediment contained in a plastic liner (6.6-cm internal diameter) plus about 0.2 m (without a plastic liner) in the core catcher (Fig. 2). The core catcher is a device at the bottom of the core barrel that prevents the core from sliding out when the barrel is being retrieved from the hole. In certain situations (e.g., when coring gas-charged sediments that expand while being brought on deck) recovery may exceed the 9.5-m maximum.

A recovered core is divided into 1.5-m sections that are numbered serially from the top (Fig. 2). When full recovery is obtained, the sections are numbered from 1 through 7, with the last section possibly being shorter than 1.5 m (rarely, an unusually long core may require more than seven sections). When less than full recovery is obtained, there will be as many sections as needed to accommodate the length of the core recovered; for example, 4 m of core would be divided into two 1.5-m sections and a 1-m section. If cores are fragmented (recovery less than 100%), sections are numbered serially and intervening sections are noted as void, whether shipboard scientists believe that the fragments were contiguous *in situ* or not. In rare cases a section less than 1.5 m may be cut to preserve features of interest (e.g., lithological contacts).

By convention, material recovered from the core catcher is placed below the last section when the core is described, and labeled core catcher (CC); in sedimentary cores, it is treated as a separate section. The core catcher is placed at the top of the cored interval in cases where material is recovered only in the

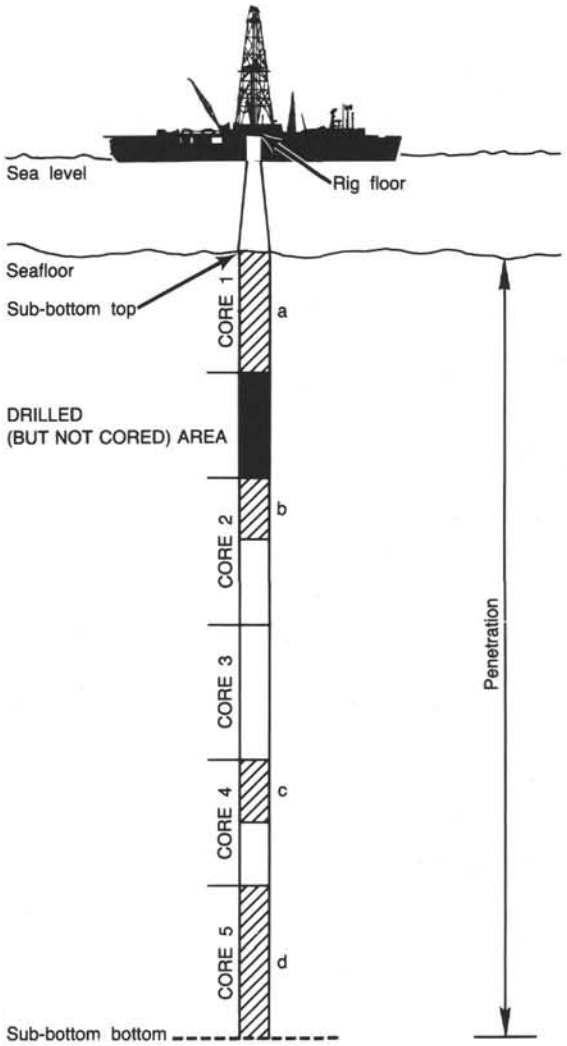

Figure 1. Diagram of terms used to discuss coring operations and core recovery.

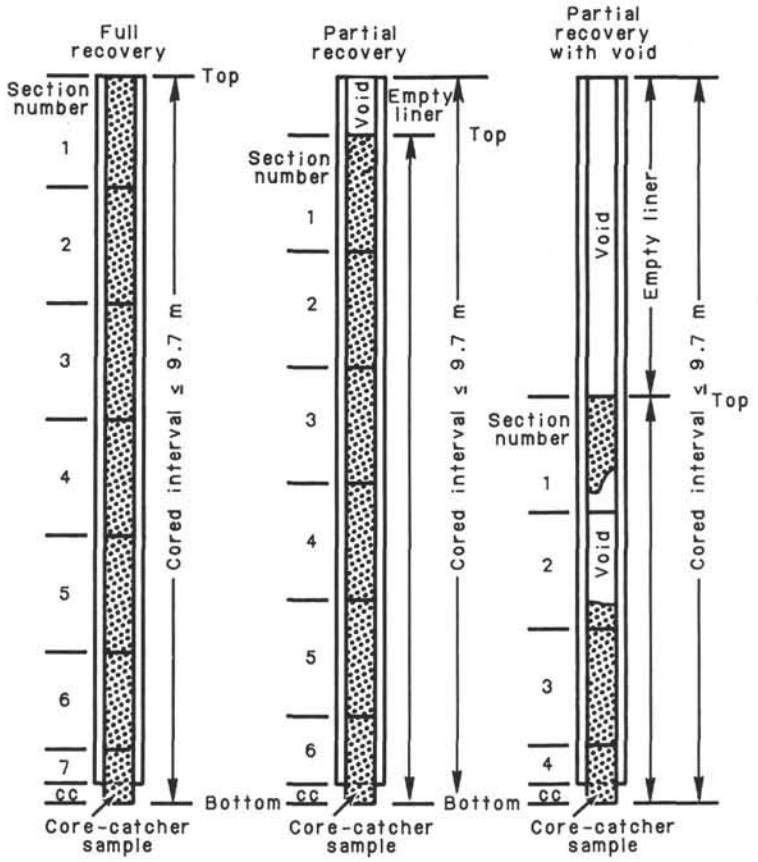

Figure 2. Diagram showing procedure used in cutting and labeling recovered core sections.

core catcher. However, information supplied by the drillers or by other sources may allow for more precise interpretation as to the correct position of core-catcher material within an incompletely recovered cored interval.

Recovered basement rock (e.g., basalt, gabbro, peridotite, or serpentinite, etc.) core is also cut into 1.5-m sections that are numbered serially; however, each piece of rock is then assigned a number. Fragments of a single piece are assigned a single number, and individual fragments are identified alphabetically. The core-catcher sample is placed at the bottom of the last section and is treated as part of the last section, rather than separately. Scientists completing visual core descriptions describe each lithologic unit, noting core and section boundaries only as physical reference points.

When, as is usually the case, the recovered core is shorter than the cored interval, the top of the core is equated with the top of the cored interval by convention, to achieve consistency in handling analytical data derived from the cores. Samples removed from the cores are designated by distance measured in centimeters from the top of the section to the top and bottom of each sample removed from that section. In curated hard rock sections, sturdy plastic spacers are placed between pieces that do not fit together to protect them from damage in transit and in storage; therefore, the centimeter interval noted for a hard-rock sample has no direct relationship to that sample's depth within the cored interval, but is only a physical reference to the location of the sample within the curated core.

A full identification number for a sample consists of the following information: leg, site, hole, core number, core type, section number, piece number (for hard rock), and interval in centimeters measured from the top of section. For example, a sample identification of "127-794A-10R-1, 10–12 cm" would be interpreted as representing a sample removed from the interval between 10 and 12 cm below the top of Section 1, Core 10 (R designates that this core was taken with the rotary core barrel) of Hole 794A during Leg 127.

All ODP core and sample identifiers indicate core type. The following abbreviations are used: R = Rotary Core Barrel (RCB); H = Hydraulic Piston Core (HPC; also referred to as APC, or Advanced Hydraulic Piston Core); P = Pressure Core Barrel; X = Extended Core Barrel (XCB); B = drill-bit recovery; C = center-bit recovery; I = *in-situ* water sample; S = sidewall sample; W = wash-core recovery; and M = miscellaneous material. APC, XCB, and RCB cores were cut on ODP Leg 127.

Core Handling

Sediments

As soon as a core is retrieved on deck, a sample is taken from the core catcher and given to the paleontological laboratory for an initial age assessment. The core is then placed on the long horizontal rack, and gas samples may be taken by piercing the core liner and withdrawing gas into a vacuum tube. Voids within the core are sought as sites for gas sampling. Some of the gas samples are stored for shore-based study, but others are analyzed immediately as part of the shipboard safety and pollution-prevention program. Next, the core is marked into section lengths, each section is labeled, and the core is cut into sections. Interstitial water (IW and BM) and organic geochemistry (OG) samples are then taken. In addition, some headspace gas samples are scraped from the ends of cut sections on the catwalk and sealed in glass vials for light hydrocarbon analysis. Each section is

then sealed at the top and bottom by gluing on color-coded plastic caps, blue to identify the top of a section and clear for the bottom. A yellow cap is placed on the section ends from which a whole-round sample has been removed. The caps are usually attached to the liner by coating the end liner and the inside rim of the cap with acetone, and then the caps are taped to the liners.

The cores then are carried into the laboratory, where the sections are again labeled, using an engraver to permanently mark the full designation of the section. The length of the core in each section and the core-catcher sample are measured to the nearest centimeter; this information is logged into the shipboard CORELOG data-base program.

Next, the whole-round sections from APC and XCB cores are run through the Multisensor Track (MST). This includes the GRAPE (gamma-ray attenuation porosity evaluator) and *P*-wave logger devices, which measure the bulk density, porosity, and sonic velocity, and also includes a meter that determines the volume magnetic susceptibility. After the core has equilibrated to room temperature (approximately 3 hr), thermal-conductivity measurements are performed, and the cores are split.

Cores of relatively soft material are split lengthwise into working and archive halves. The softer cores are split with a wire or saw, depending on the degree of induration. Harder cores are split with a band saw or diamond saw. The wire-cut cores were split from the bottom to top, so investigators should be aware that older material could have been transported up the core on the split face of each section.

The working half of the core is sampled for both shipboard and shore-based laboratory studies. Each extracted sample is logged into the sampling computer data-base program by the location and the name of the investigator receiving the sample. Records of all removed samples are kept by the curator at ODP. The extracted samples are sealed in plastic vials or bags and labeled. Samples are routinely taken for shipboard physical property analysis. These samples are subsequently used for calcium carbonate determinations (coulometric analysis) and the data are reported in the site chapters.

The archive half is described visually. Smear slides are made from samples taken from the archive half, and are supplemented by thin-sections taken from the working half. Sections from the archive half that do not show evidence of drilling disturbance are run through the cryogenic magnetometer. The archive half is then photographed with both black-and-white and color film, a whole core at a time. Close-up photographs (black-and-white) are taken of particular features for illustrations in the summary of each site.

Both halves of the core are then put into labeled plastic tubes, sealed, and transferred to cold-storage space aboard the drilling vessel. At the end of the leg, the cores are transferred from the ship in refrigerated air-freight containers to cold storage at the Gulf Coast Repository at the Ocean Drilling Program, Texas A&M University, College Station, Texas.

Igneous and Metamorphic Rocks

Igneous and metamorphic rock cores are handled differently from sedimentary cores. Once on deck, the core catcher is placed at the bottom of the core liner and total core recovery is calculated by shunting the rock pieces together and measuring to the nearest centimeter; this information is logged into the shipboard core-log data-base program. The core is then cut into 1.5-m-long sections and transferred into the lab.

The contents of each section are transferred into 1.5-m-long sections of split core liner, where the bottom of oriented pieces (i.e., pieces that clearly could not have rotated top to bottom about a horizontal axis in the liner) are marked with a red wax pencil. This is done to ensure that orientation is not lost during the splitting and labeling process. The core is then split into archive and working halves. A plastic spacer is used to separate individual pieces and/or reconstructed groups of pieces in the core liner. These spacers may represent a substantial interval of no recovery. Each piece is numbered sequentially from the top of each section, beginning with number 1; reconstructed groups of pieces are assigned the same number, but are lettered consecutively. Pieces are labeled only on external surfaces. If the piece is oriented, an arrow is added to the label pointing to the top of the section.

The working half of the hard-rock core is then sampled for shipboard laboratory studies. Records of all samples are kept by the curator at ODP. Minicore samples are routinely taken for physical properties and magnetic studies. Some of these samples are later subdivided for X-ray fluorescence (XRF) analysis and thin-sectioning, so that as many measurements as possible are made on the same pieces of rock. At least one minicore is taken per lithologic unit when recovery permits, generally from the freshest areas of core. Additional thin-sections, X-ray diffraction (XRD) samples, and XRF samples are selected from areas of particular interest. Samples for shore-based studies are selected in a sampling party held after drilling has ended.

The archive half is described visually, then photographed with both black-and-white and color film, one core at a time. Both halves of the core are then shrink-wrapped in plastic to prevent rock pieces from vibrating out of sequence during transit, put into labeled plastic tubes, sealed, and transferred to cold-storage space aboard the drilling vessel.

VISUAL CORE DESCRIPTION

Sediment "Barrel Sheets"

The core description forms (Fig. 3), or "barrel sheets", summarize the data obtained during shipboard analysis of each sediment core. The following discussion explains the ODP conventions used in compiling each part of the core description forms and the exceptions to these procedures adopted by Leg 127 scientists.

Sediments and Pyroclastic Deposits

Shipboard sedimentologists were responsible for visual core logging, smear-slide analyses, and thin-section descriptions of sedimentary and pyroclastic material. Some analytical grain-size data and mineral composition, determined by XRD, was used to augment the visual core descriptions. Biostratigraphic (age), geochemical ($CaCO_3$, C_{org}), magnetic, and physical property (index properties, acoustic velocity, formation factor, and thermal conductivity) data, supplied by other groups, were integrated with the sedimentological information. This information provided the basis for core barrel log descriptions in this volume.

Core Designation

Cores are designated using leg, site, hole, core number, and core type as discussed in a preceding section (see "Numbering of Sites, Holes, Cores, and Samples" section, this chapter). The cored interval is specified in terms of meters below sea level (mbsl) and meters below seafloor (mbsf). On the basis of drill-pipe measurements (dpm), reported by the SEDCO coring technician and the ODP operations superintendent, depths are corrected for the height of the rig floor dual elevator stool above sea level to give true water depth and the correct mbsl.

Graphic Lithology Column

The lithology of the recovered material is represented on the core description forms (barrel sheets) by a single symbol or by a group of two or more symbols (see Fig. 4) in the column titled "Graphic Lithology."

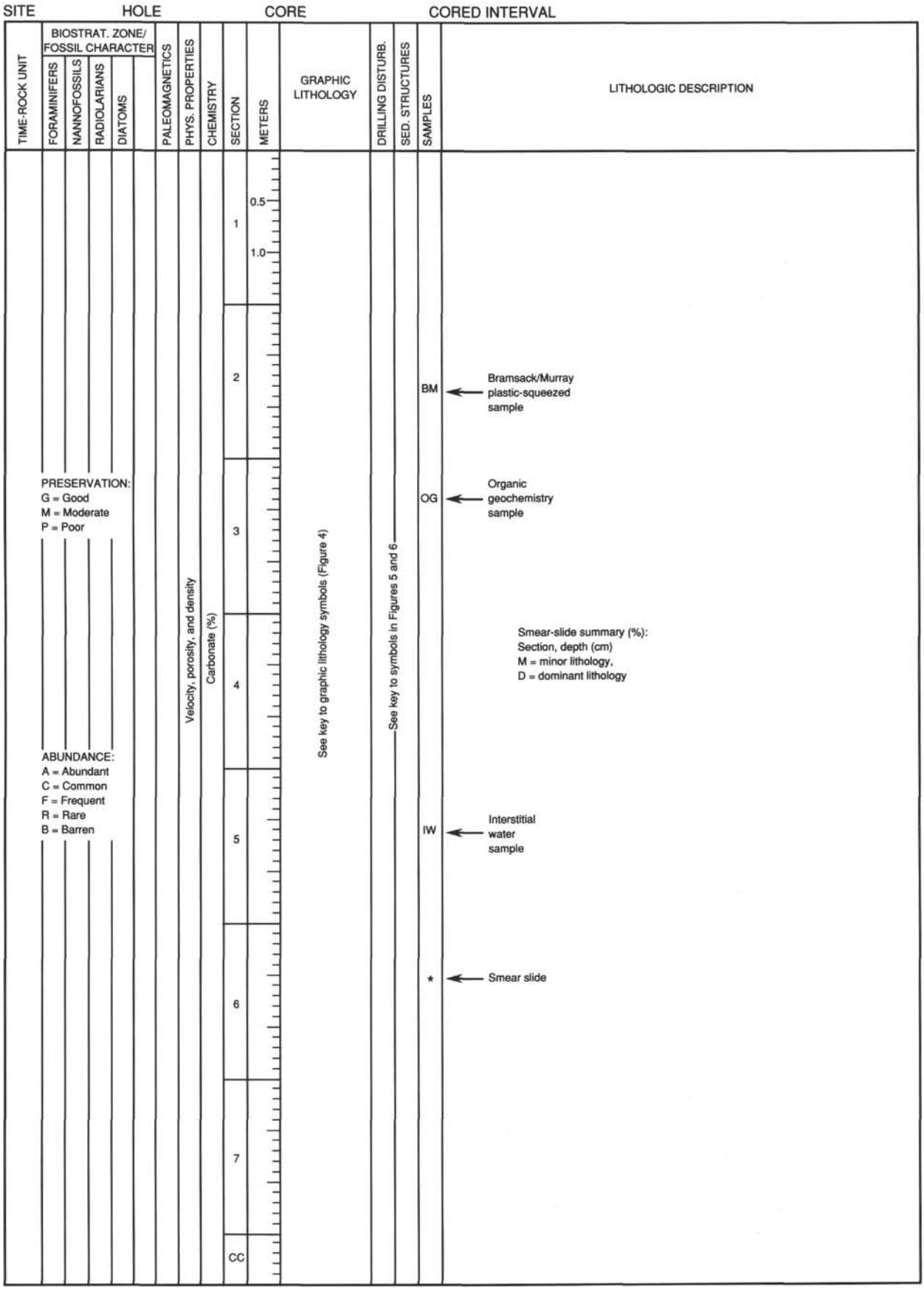

Figure 3. Core description form ("barrel sheet") used for sediments and sedimentary rocks.

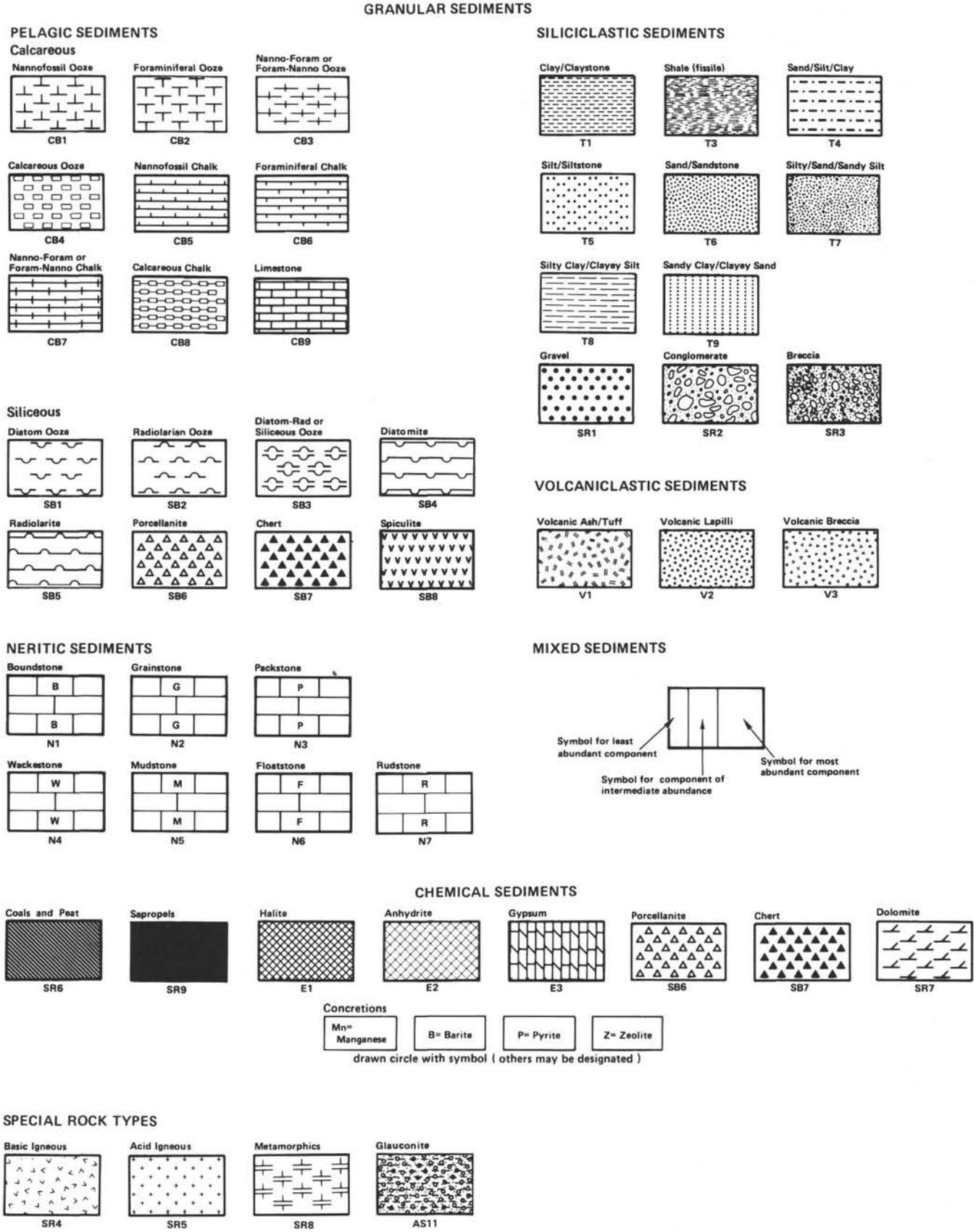

Figure 4. Key to symbols used in the "graphic lithology column" on the core description form shown in Figure 3.

Where the sediment or sedimentary rock is essentially a homogeneous mixture of the two constituents, the interval is split by a solid line, although each lithology is represented by its own symbol. In a mixed biogenic-siliciclastic sediment such as diatom-rich clay, the terrigenous constituent is noted on the right, the biogenic constituent(s) on the left side of the column, in proportions approximately equal to their respective abundances in the sediment.

In an interval composed of two or more sediment types that are too finely interbedded for each layer to be depicted individually, the relative abundances of the lithotypes are shown graphically by dashed lines that vertically divide the interval into appropriate fractions.

The numerous thin ash layers in Pliocene-Pleistocene sediments recovered during Leg 127 are significant; however, owing to space limitations on barrel sheets only the thicker of these ash layers (above 5 cm in thickness) are illustrated in the stratigraphic columns. Thinner individual horizons are noted in the barrel sheet lithologic descriptions. For additional information on these ash layers, the reader is referred to the shipboard visual description logs, core photographs, and the smear-slide descriptions.

The following notations have been used on the barrel sheets to indicate the following sedimentary types/zones: PH = Phosphatic Claystone, G = Glauconite, A = Opal-A, CT = Opal-CT, and Q = Quartz.

As noted during previous legs, intercalations of sedimentary material and igneous rocks occurred in some core sections. Where this occurred, the igneous petrologists described the igneous section and recorded results under "Hard Rock Core Description Forms."

Sediment Disturbance

Sediment disturbance is illustrated in the "Drilling Disturbance" column on the core description form (using the symbols in Fig. 5). Blank regions indicate a lack of drilling disturbance. Drilling disturbance is recognized for soft and firm sediments using these categories.

1. Slightly deformed: bedding contacts are slightly bent.
2. Moderately deformed: bedding contacts have undergone extreme bowing.
3. Highly deformed: bedding is completely disturbed, sometimes showing symmetrical diapir-like or flow structures.
4. Soupy: intervals are water saturated and have lost all aspects of original bedding.

The degree of fracturing in indurated sediments and igneous rocks is described using the following categories:

1. Slightly fractured: core pieces are in place and contain little drilling slurry or breccia;
2. Moderately fragmented: core pieces are in place or partly displaced, but original orientation is preserved or recognizable (drilling slurry may surround fragments);
3. Highly fragmented: pieces are from the interval cored and probably in correct stratigraphic sequence (although they may not represent the entire section), but original orientation is completely lost;
4. Drilling breccia core pieces have lost their original orientation and stratigraphic position and may be mixed with drilling slurry.

Sedimentary Structures

In sediment cores, natural structures and structures created by the coring process can be difficult to distinguish from one another. Natural structures observed are indicated in the "Sedimentary Structure" column of the core description form. The symbols used to describe the primary biogenic and physical sedimentary structures, and secondary structures such as microfaults, dewatering veinlets, and mineral-filled fractures, are given in Figure 5.

Color

Colors were determined by comparison with the Munsell and Geological Society of America soil-color charts. Colors were determined immediately after the cores were split because chemical changes may occur when deep-sea sediments are exposed to the atmosphere. Information on core colors is given in the text of the "Lithologic Description" on the core description forms, and where appropriate in Site chapters.

Samples

The position of samples taken from each core for shipboard analysis is indicated in the "Samples" column on the core-description form. The symbol "*" indicates the location of samples used for smear-slide analysis. The symbols "TS," "XRD," and "XRF" indicate the location of samples for shipboard thin-sections, XRD analysis, and XRF analysis, respectively. The symbols IW (and BM), OG, and PP, designate the location of samples for whole-round interstitial water geochemistry, frozen organic geochemistry, and physical properties, respectively.

Although not indicated in the "Samples" column, positions of samples for routine physical-properties and geochemical analysis are indicated by a dot and analytical results are presented in the "Physical Properties" and in the "Chemistry" columns, respectively. Paleomagnetic results are indicated in the "Paleomagnetics" column.

Shipboard paleontologists generally base their age determinations on core-catcher samples, although additional samples from other parts of the core may be examined when required. Examination of such samples may lead to the recognition of zonal boundaries in the core; these are also indicated in the appropriate column. All paleontological sample locations are indicated, even if they are barren.

Smear-Slide Summary

A table summarizing data from smear slides and thin sections (where available) appears on each core description form. The table includes information on section and interval from which the sample was taken, whether the sample represents a dominant ("D") or a minor ("M") lithology in the core, and the estimated percentages of sand, silt, and clay, together with all identified components. The term "Glass" has been used to define all vitric pyroclasts including volcanic shards and pumice.

Lithologic Description—Text

The lithologic description that appears on each core description form (barrel sheet) consists of two parts: (1) a heading that lists all the major sediment types (see "Sediment Classification" section, this chapter) observed in the core; and (2) a more detailed description of these sediments, including data on color, location in the core, significant features, etc. In cases where there are thin beds of minor lithology, a description including location information is included in the text, but the beds may be too thin (<10 cm) to appear in the graphic lithology column.

Paleontological Data

Microfossil abundance, preservation, and zone assignment, as determined by the shipboard paleontologists, appear on the core description form under the heading "Biostrat. Zone/Fossil Character." The chronostratigraphic unit, as recognized on the basis of paleontological results, is shown in the "Time-Rock

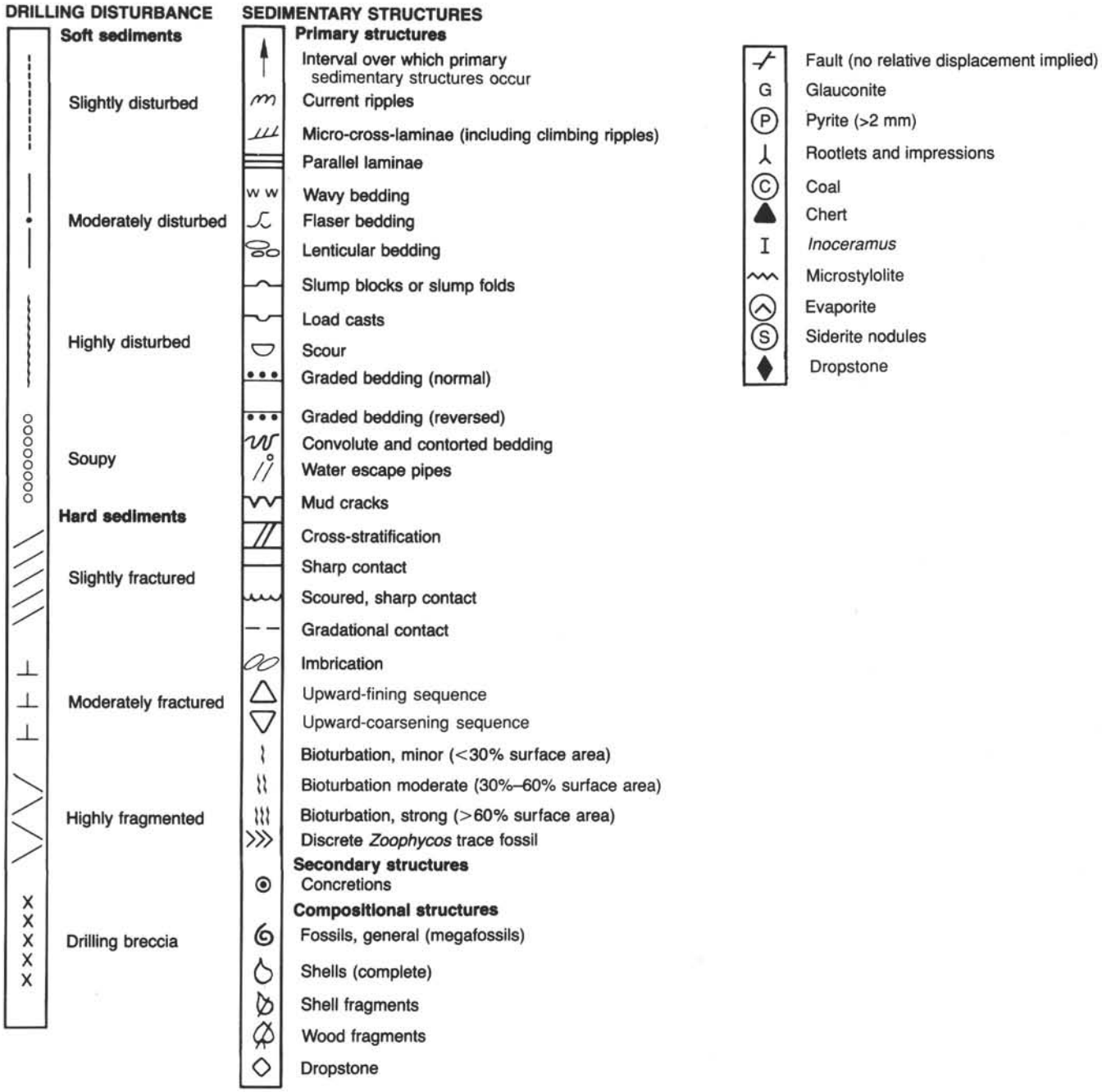

Figure 5. Symbols used for drilling deformation and sedimentary structure on core description form shown in Figure 3.

Unit" column. Detailed information on the zonations and terms used to report abundance and preservation is presented in the "Biostratigraphy" section (this chapter).

Paleomagnetic, Physical Property, and Chemical Data

Columns are provided on the core description form to record paleomagnetic results (normal, reversed or indeterminate polarity, shown as "N," "R," or "INT," respectively), physical properties values (density, porosity, and velocity) and chemical data (percentages of $CaCO_3$ and total organic carbon determined using the Coulometrics analyzer). Additional information on shipboard procedures for collecting these types of data appears in the "Paleomagnetism," "Physical Properties," and "Inorganic Geochemistry" sections (this chapter).

CLASSIFICATION OF SEDIMENTS AND PYROCLASTIC MATERIALS

The classification scheme for sediments and pyroclastic materials adopted during Leg 127 is modified slightly from the classification recommended in the ODP "Handbook for Shipboard Sedimentologists" (Mazzullo and Graham, 1988, p. 48). The classification is primarily descriptive; it uses composition and texture as the principal criteria to define lithology (Fig. 6, Table 1). A principal name is assigned on the basis of a component that makes up 60% or more of the sediment or pyroclastic material. The names of components that make up less than 60% of the sediment or rock are used as modifiers of the principal name. This classification scheme differs from some prior

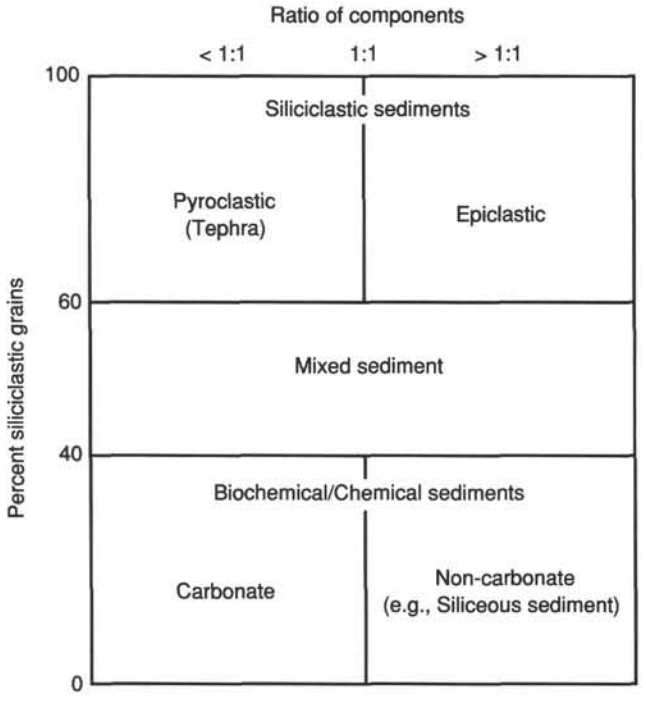

Figure 6. Diagram showing classes of granular sediments and pyroclastic materials. Modified from Mazzullo and Graham (1988), p. 47.

DSDP and ODP classifications in the specific use of compositional modifiers; otherwise, it mainly follows the classification of Mazzullo and Graham (1988, p. 48).

Data for classifying sedimentary and pyroclastic materials come primarily from shipboard visual inspection and analysis of smear slides using the petrographic microscope. These analyses yield qualitative data (e.g., kinds of biogenic remains) and semi-quantitative optical estimates of particle characteristics (e.g., grain size, relative abundance of mineral constituents, and biogenic remains). Smear-slide data may differ from the results of purely quantitative analyses of grain size, carbonate content, and mineralogy. Selected samples are analyzed by thin-section petrography, yielding more accurate data on particle composition.

Texture and Composition

"Clay" is used as a textural term for epiclastic or pyroclastic material less than 4 μm in size without regard to origin. For coarser grained epiclastic materials, we use the standard size terms (silt, sand, gravel) of Wentworth (1922), and then indicate composition with a modifier. For coarser-grained pyroclastic materials, identified by such objective criteria as the presence of glass shards, pumice, and euhedral crystals, we use the size terms ash, lapilli, and block-bomb (Table 2). Biogenic components are not classified according to grain size. Thus, a sediment with 50% silt-sized nannofossils and 50% terrigenous clay is called a nannofossil clay, not a nannofossil silt. The shipboard sedimentologists have chosen to use this classification to (1) maintain an internal consistency in the naming of intermediate mixtures of siliciclastic and chemical/biochemical components, and (2) provide simple descriptive modifiers that indicate the important components and their relative abundance in the deposits.

Induration

Determination of induration is subjective. For calcareous sediments and calcareous sedimentary rocks, three classes of induration or lithification are recognized (Gealy et al., 1971): (1) soft = ooze, which has little strength and is readily deformed under the pressure of a finger or the broad blade of a spatula; (2) firm = chalk, which is partially lithified, readily scratched with a fingernail or the edge of a spatula; and (3) hard = well-lithified and cemented limestone or dolomite that is difficult or impossible to scratch with a fingernail. The terms ooze and chalk are applied to deposits composed dominantly of the remains of carbonate pelagic organisms.

The term ooze is also used for soft siliceous sediments. Firm siliceous sediment is called radiolarite, diatomite, or spiculite, depending upon the principal kinds of siliceous organisms that make up the sediment. Extremely well-lithified siliceous sediment is called chert.

For siliciclastic sediment, lithified varieties are generally indicated by addition of the suffix "-stone" to the name for soft materials. For gravel, the lithified equivalent is conglomerate or breccia.

Rules for Classification

1. Principal Names. The principal name is determined by the component that makes up at least 60% of the sediment or pyroclastic material, except for subequal mixtures of siliciclastic and chemical/biochemical material (Fig. 6). The principal names for major classes of sediments and pyroclastic materials are as follows:

A. Siliciclastic Sediments and Rocks. If the total of siliciclastic components is greater than 60%, the principal name is determined by the relative proportions of sand-, silt-, and clay-size particles when plotted on a modified Shepard (1954) classification diagram (Fig. 7). Examples of siliciclastic sediment principal names are clay, silt, and sand. Equivalent names for consolidated rocks are claystone, siltstone, and sandstone. Names for pyroclastic materials are derived from Table 2, after Fisher and Schmincke (1984). Examples of pyroclastic principal names are ash, lapillus, and block-bomb. Equivalent names for consolidated pyroclastic rocks are tuff, lapilli tuff, and breccia. Modifiers for principal names of pyroclastic materials are "vitric" (for glass), "volcanic-lithic" (for polycrystalline material), and "crystal" (for unit crystals) (see item 3 below). These modifiers are placed immediately before the textural name. The textural term forms the principal name, and compositional terms form major modifiers.

B. Chemical/Biochemical Sediments and Rocks. If the total of calcareous, pelagic skeletal components is greater than 60%, the principal name is ooze, chalk, or limestone, depending upon the state of induration. If the total of siliceous, pelagic skeletal components is greater than 60%, the principal name is ooze, radiolarite, diatomite, spiculite, or chert, depending upon composition and state of induration. Carbonate sediments composed of nonskeletal grains or skeletal grains other than the remains of pelagic organisms are given principal names on the basis of the textural classification of Dunham (1962), as modified by Embry and Klovan (1972). Examples are packstone, wackestone, and floatstone. Other chemical/biochemical sediments are named on the basis of major-component composition, e.g., phosphorite and gypsum.

C. Mixed sediments. In mixtures of siliciclastic and chemical/biochemical sediments where neither component exceeds 60%, we use the convention that the principal name will consist of two parts: (1) the name of the major fossil(s) or other chemical/biochemical grains, hyphenated if necessary with the least-common fossil listed first, followed by (2) the textural name appropriate for the epiclastic/pyroclastic components. For example, if nannofossils form 40%–60% of a sediment that contains nothing else but clay, then the name is nannofossil clay, even if nannofossils are somewhat more abundant than clay.

Table 1. Outline of classification scheme for sediments and pyroclastic materials. Modified from Mazzullo and Graham (1988, Table 1, p. 49).

	Sediment class	Major modifiers	Principal names	Minor modifiers
CHEMICAL/BIOCHEMICAL	Carbonates	1. composition of carbonate grains present in major amounts	ooze (soft, pelagic) chalk (firm, pelagic) limestone (hard, pelagic)	1. composition of carbonate grains present in minor amounts
		2. texture of clastic grains present in major amounts	boundstone grainstone packstone wackestone mudstone floatstone rudstone	2. texture of clastic grains present in minor amounts
	Siliceous sediments	1. composition of siliceous biogenic grains	ooze (soft, pelagic) radiolarite (firm) diatomite (firm) spiculite (firm) chert (hard)	1. composition of siliceous biogenic grain present in minor amounts
		2. texture of clastic grains present in major amounts		2. texture of clastic grains present in minor amounts
	Other	texture of clastic grains present in major amounts	phosphorites gypsum, etc.	texture of clastic grains present in minor amounts
SILICICLASTIC	Epiclastic sediment	1. composition of all grains present in major amounts	gravel sand silt clay	1. composition of all grains present in minor amounts
		2. grain fabric (gravels only)		2. texture and composition of siliciclastic grains present as matrix in coarse sediments
	Pyroclastic deposits	1. composition of all pyroclasts present in major amounts	breccia lapillus ash	1. composition of all pyroclasts present in minor amounts
		2. composition of all other grains present in major amounts		2. composition of all other grains present in minor amounts
		3. texture of clastic grains present in major amounts		3. texture of clastic grains present in minor amounts
MIXED	Mixed sediments	1. composition of all grains present in major amounts	all grains	1. composition of mixed sediments present in minor amounts
		2. texture of clastic grains present in major amounts		2. texture of clastic grains present in minor amounts

2. Major modifier status is characterized by 25%–50% of a component. Examples of major modifiers for different classes of sediments and pyroclastic materials are:

A. Siliciclastic deposits: silty, clayey, sandy, vitric-sandy, ashy, etc.

B. Carbonate sediments: nannofossil, foraminiferal, bioclastic, oolitic, etc.

C. Biogenic siliceous sediments: diatomaceous, radiolarian, and spiculitic.

D. Other chemical/biochemical sediments: phosphatic, glauconitic, etc.

Note that for sediments containing from 40% to 60% chemical/biochemical material, this rule is partly redundant with rule 1C.

3. Minor modifier status is characterized by 10%–25% of a component. Examples are nannofossil clay, diatomaceous clay, and vitric clay.

Table 2. Classification of pyroclastic deposits. (From Fisher and Schmincke, 1984, p. 90.)

Clast size	Pyroclast	Pyroclastic deposit: Mainly unconsolidated: tephra	Pyroclastic deposit: Mainly consolidated: pyroclastic rock
	Block, bomb	Agglomerate, bed of blocks or bomb, block tephra	Agglomerate, pyroclastic breccia
64 mm			
	Lapillus	Layer, bed of lapilli or lapilli tephra	Lapillistone
2 mm			
	Coarse ash grain	Coarse ash	Coarse (ash) tuff
1/16 mm			
	Fine ash grain (dust grain)	Fine ash (dust)	Fine (ash) tuff (dust tuff)

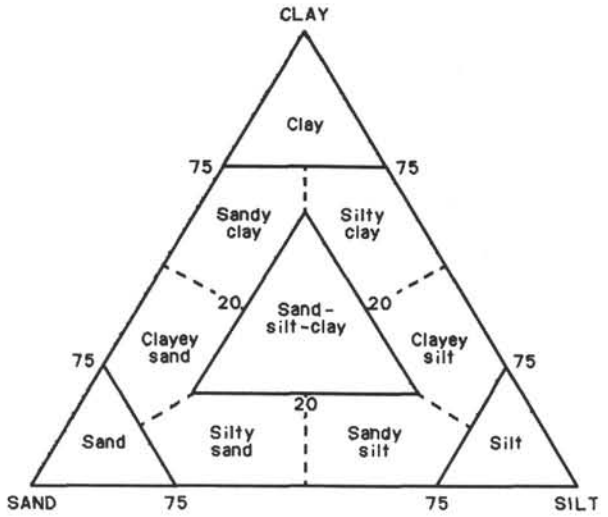

Figure 7. Ternary diagram showing principal textural names for siliciclastic sediment. From Shepard, 1954.

4. An optional modifier status is characterized by 5%–10% of an unusual, important component (e.g., phosphatic and glauconitic grains, bioclasts, zeolite, granules, large foraminifers) and can be indicated with the component name hyphenated with the word "bearing." Example: zeolite-bearing clay.

5. The most abundant accessory component appears closest to the principal name. Major and minor modifiers are listed in order of decreasing abundance to the left of the principal name.

Examples: foraminifer-bearing diatomaceous clay
(10%) (30%) (60%)

radiolarian-bearing clayey diatomaceous ooze
(5%) (20%) (75%)

6. The classification of true chemical/diagenetic sediments adheres to the nomenclature described in the Mazzullo and Graham (1988, p. 56–57). Most significant for Leg 127 are diagenetic siliceous rocks (porcellanite and chert), diagenetic carbonates (calcite, dolomite, ankerite), manganese or pyrite-bearing sediments, and *in-situ* phosphate concretions.

BIOSTRATIGRAPHY

Biostratigraphic Framework

Figure 8 summarizes the general correlation of planktonic microfossil zones, datum levels, and the magnetic polarity reversal record for the Miocene to Quaternary in the Japan Sea. Datum levels for each microfossil group are listed in Tables 3, 4, 5, and 6.

Age assignments for Leg 127 were based mainly on core-catcher samples. Additional core samples were studied when the core-catcher samples were either barren or restricted to narrow time intervals or where boundaries or unconformities occurred. Sample locations within cores, preservation, and abundance for each fossil group are recorded on ODP paleontology and biostratigraphy data forms, and zones, abundance, and preservation are indicated on the barrel sheets.

Diatoms

The zonations described in Koizumi (1985) and Koizumi and Tanimura (1985) were used in part as modified by Akiba and Yanagisawa (1985) based on the taxonomic revisions of Akiba (1985). Table 3 summarizes the lower Miocene to Quaternary diatom zonal datum levels that were used to date Leg 127 cores.

Samples were disaggregated in water and a dilute solution of 10% hydrogen peroxide. Carbonate nodules and concretions were treated with 10% hydrochloric acid. Smear slides were prepared using Hyrax or Pleurax as a mounting medium. Relative abundances reflect percentage estimates of diatom valves within all material on the slide. The following convention was used:

A = Abundant, >50%.
C = Common, 25%-50%.
F = Few, 1%-25%.
R = Rare, <1%.
B = Barren, no diatoms present.

Preservation of diatoms was classified into three major categories based on the presence of complete or broken, thinly silicified or heavily silicified frustules as follows:

Good: well preserved with numerous delicate frustules.
Moderate: some thinly silicified frustules present.
Poor: only heavily silicified frustules present.

Calcareous Nannofossils

The calcareous nannofossil zonations used at all Leg 127 sites (Table 4) follow Bukry (1978) and Rahman and Roth (1989). The absolute ages of the nannofossil datum levels (i.e., First Appearance Datum = FAD and Last Appearance Datum = LAD) are adopted from Berggren et al. (1985a, b) and Rahman and Roth (1989).

Smear slides were prepared using standard procedure (Perch-Nielsen, 1985) without any chemical or ultrasonic treatment. Relative abundance and state of preservation of nannofossils were determined under light microscope in random traverses at magnification of about 1560×. The following categories of relative abundance were distinguished:

A = Abundant (more than 10 specimens/field of view).
C = Common (between 1 and 10 specimens/field of view).
F = Few (1 specimen/2–10 fields of view).
R = Rare (1 specimen/more than 10 fields of view).
B = Barren (no specimens present).

The preservation categories based on tropical and subtropical nannofossil assemblages Roth (1974) are not applicable to the nannofossils in the Japan Sea because most of the delicate species used in Roth (1974) to describe the preservation are absent. A simplified scheme was used to characterize the state of preservation of calcareous nannofossils as summarized as follows:

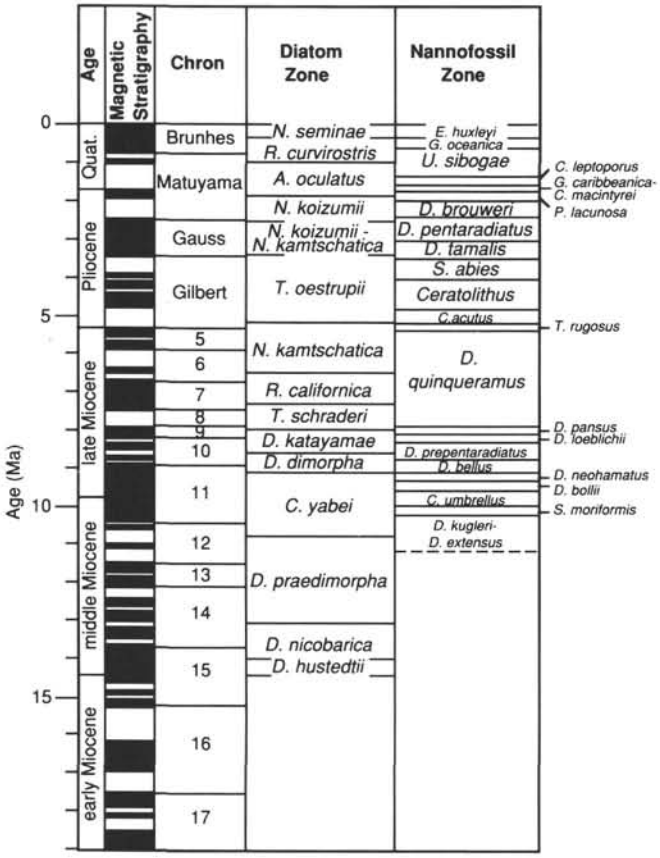

Figure 8. Biostratigraphic framework used on Leg 127.

G = Good preservation, individual specimens shows little or no effect of dissolution or overgrowth, central structures of the coccoliths are well preserved.

M = Moderate preservation, moderately etched with slight to moderate overgrowth, central opening of the coccoliths are enlarged and the outer margins serrated due to etching, some shields of the placoliths are separated.

P = Poor preservation, strongly etched with moderate to strong overgrowth. Small coccoliths and *Sphenolithus* are mostly broken. The arms of discoasters are thicker due to overgrowth.

Foraminifers

The cold-water planktonic foraminifer biofacies of upper middle Miocene through Quaternary sequences from the Japan Sea could not be described using a previously defined zonation. The absence of globorotalid species made impossible recognition of zones defined by Jenkins and Srinivasan (1986), and sporadic occurrences made impossible assignment of samples to the assemblage zones of Maiya et al. (1976) for the Oga Peninsula or the coiling direction zones of Lagoe and Thompson (1988) for the California borderland and North Pacific Ocean.

Lower middle Miocene planktonic foraminifer biofacies are temperate and contain several species with short ranges; however, none are used in previously defined warm-water zonations (i.e., Blow, 1969; Saito, 1963; Asano et al., 1969). Correlations of planktonic foraminifer datum levels to magnetic polarity stratigraphy summarized by Berggren et al. (1985a, b) were adapted for this study, with modification of dates of first (FAD) and last (LAD) appearances of high-latitude species as noted in Table 5.

Table 3. Diatom datum levels for the Miocene to Pleistocene.

Event	Species	Age (Ma)	References
LAD	*Rhizosolenia curvirostris*	0.30–0.35*	(1)
LAD	*Actinocyclus oculatus*	0.93–1.33*	(1)
FAD	*Pseudoeunotia doliolus*	1.89–2.00*	(1)
LAD	*Neodenticula kamtschatica*	2.50–2.58*	(1)
FAD	*Neodenticula koizumii*	3.36–3.70*	(1)
FAD	*Nitzchia jouseae*	4.50*	(1)
FAD	*Thalassiosira oestrupii*	5.10*	(2)
LAD	*Rouxia californica*	5.10	(3)
LAD	*Nitzschia miocenica*	5.55*	(4), (3)
FAD	*Neodenticula kamtschatica*	6.40–6.60*	(6)-(5), (3)
LAD	*Thalassionema schraderi*	7.20	(6)
LAD	*Thalassiosira burckliana*	7.20*	(4), (3), (6)
LAD	*Denticulopsis katayamae*	7.90–8.00	(6)-(3)
LAD	*Denticulopsis dimorpha*	8.50	(3), (6)
FAD	*Denticulopsis katayamae*	8.75–8.90	(3)-(6)
FAD	*Denticulopsis dimorpha*	8.90–9.00	(3)-(6)
LAD	*Denticulopsis praedimorpha*	9.60	(6)
RDD	*Denticulopsis praedimorpha*	10.65	(6)
FAD	*Denticulopsis praedimorpha*	12.90–13.30	(6)-(3)
RID	*Denticulopsis hustedtii*	13.85–14.00	(6)-(3)
RDD	*Denticulopsis hyalina*	13.85–14.00	(6)-(3)
FAD	*Denticulopsis hustedtii*	14.30–14.50	(6)-(3)
FAD	*Denticulopsis hyalina*	4.60–14.85	(6)-(3)
FAD	*Denticulopsis lauta*	15.60–15.70	(6)-(3)
FAD	*Denticulopsis praelauta*	16.00	(3), (6)
FAD	*Actinocyclus ingens*	17.60–17.90	(6)-(3)

LAD = top of species range or last appearance datum
FAD = base of species range or first appearance datum
RDD = rapid decrease datum of species
RID = rapid increase datum of species
* = direct paleomagnetic tie
(1) Koizumi and Tanimura (1985)
(2) Burckle, Keigwin, and Opdyke (1982)
(3) Koizumi (1985)
(4) Burckle (1977)
(5) Burckle and Trainer (1979)
(6) Oda (1986)

Benthonic foraminifers were used to define paleodepths (Matoba, 1984 and references therein). Benthonic depth zones are defined as in Ingle (1973):

Upper Bathyal	150–500 m
Upper Middle Bathyal	500–1500 m
Lower Middle Bathyal	1500–2500 m
Lower Bathyal	2500–4000 m

Samples were oven dried at 60°C, disaggregated either in a 1% Calgon solution (sodium metaphosphate) or 10% hydrogen peroxide, and washed through a sieve of 63-μm openings. Abundance of planktonic foraminifers was estimated in samples normalized to 20 cm^3 in volume using the following categories:

A = Abundant, >1000 tests in the residue.
C = Common, 100–999 tests in the residue.
F = Few, 10–99 tests in the residue.
R = Rare, 1–9 tests in the residue.
B = Barren, no tests present.

Preservational characteristics were divided into three categories based on the extent of breakage and the proportion of delicate to robust tests:

Good: <10% of specimens broken, and delicate specimens are common.

Moderate: <30% of specimens broken, and delicate specimens are rare.

Table 4. Calcareous nannofossil zones and datum levels used at all sites of Leg 127.

Event	Species	Age (Ma)	References	Zone/subzone
FAD	*E. huxleyi*	0.275	(1)	*E. huxleyi*
LAD	*P. lacunosa*	0.47	(1)	*G. oceanica*
FAD	*G. oceanica*	1.35	(2)	*U. sibogae*
LAD	*Cal. macintyrei*	1.55	(2)	*Cal. leptoporus*
FAD	*G. caribbeanica*	1.68	(2)	*G. caribbeanica*
				Cal. macintyrei
LAD	*D. brouweri*	1.95	(2)	*P. lacunosa*
LAD	*D. pentaradiatus*	2.35	(2)	*D. brouweri*
LAD	*D. tamalis*	2.65	(1)	*D. pentaradiatus*
LAD	*S. neoabies*	3.51	(2)	*D. tamalis*
FAD	*P. lacunosa*	4.05	(2)	*S. abies*
LAD	*Cer. acutus*	4.86	(2)	*Ceratolithus*
FAD	*Cer. acutus*	5.23	(2)	*Cer. acutus*
LAD	*D. quinqueramus*	5.37	(2)	*T. rugosus*
FAD	*D. quinqueramus*	7.86	(2)	*D. quinqueramus*
				D. loeblichii
LAD	*D. neohamatus*	8.10	(2)	*D. pansus*
LAD	*D. loeblichii*	8.32	(2)	*D. loeblichii*
FAD	*D. loeblichii*	8.79	(2)	*D. prepentaradiatus*
LAD	*D. hamatus*	9.15	(2)	*D. bellus*
				D. hamatus
FAD	*D. neohamatus*	9.35	(2)	*D. neohamatus*
LAD	*D. calcaris*	9.65	(2)	*D. bollii*
FAD	*D. hamatus*	10	(1)	*Cat. umbrellus*
LAD	*D. extensus*	10.25	(2)	*S. moriformis*
FAD	*D. kugleri*	13.1	(1)	*D. kugleri*
				D. extensus
LAD	*S. heteromorphus*	14.4	(1)	*D. exilis*
FAD	*Cal. macintyrei*	?		*S. heteromorphus*
FAD	*S. heteromorphus*	17.1	(1)	*H. ampliperta*
FAD	*S. belemnos*	21.5	(1)	*S. belemnos*
				T. carinatus
FAD	*D. druggii*	23.2	(1)	*D. druggii*
LAD	*R. abisecta*	23.7	(1)	*D. deflandrei*

(1) Berggren et al. (1985)
(2) Rahman and Roth (1989)
E. = *Emiliania*, *G.* = *Gephyrocapsa*, *U.* = *Umbilicosphaera*, *Cal.* = *Calcidiscus*, *P.* = *Pseudoemiliania*, *Cer.* = *Ceratolithus*, *D.* = *Discoaster*, *S.* = *Sphenolithus*, *Cat.* = *Catinaster*, *T.* = *Triquetrorhabdulus*, *R.* = *Reticulofenestra*.

Table 5. Planktonic foraminifer datum levels for the Miocene to the Pleistocene.

Event	Species	Age (Ma)	References
LAD	*Nq. kagaensis*	1.6	(3)
LAD	*Nq. asanoi*	1.85	(3)
LAD	*Nq. continuosa*	5.2	(1)
FAD	*Nq. pachyderma*	10.2	(4)
LAD	*Gr. peripheroronda*	14.6	(2)
LAD	*Ct. parvulus*	10.2	(4)
FAD	*Ga. bulloides*	16	(4)
FAD	*Ct. parvulus*	17.6	(4)
FAD	*Gr. peripheroronda*	23	(4)

(1) Keller, Barron, and Burckle (1982)
(2) Berggren, Kent, and van Couvering (1985b)
(3) Lagoe and Thompson (1988)
(4) Kennett and Srinivasan (1983)
FAD = first appearance datum
LAD = last appearance datum
Nq. = *Neogloboquadrina*
Gr. = *Globorotalia*
Ga. = *Globigerina*
Ct. = *Catapsydrax*

Poor: samples dominated by fragments, and barren of delicate specimens.

Radiolarians

The radiolarian zonation used during Leg 127 is a modification of the zonal scheme developed by Nakaseko and Sugano (1973) for siliceous units of Japan of Miocene and early Pliocene age. Although the more detailed and generally accepted zonations for North Pacific and tropical Pacific sites outlined by Reynolds (1980) and Sanfilippo et al. (1985) would be more practical for global correlation, they were not applicable during Leg 127. Sediments containing radiolarians have been recovered from Japan Sea submarine deposits during DSDP Leg 31 (Ling, 1975), but were not successfully zoned. Most of the zonal markers used in Reynolds (1980) and Sanfilippo et al. (1985) were not found or showed inconsistent ranges due to varied states of preservation in Leg 127 sediments. Figure 9 shows the three zonal schemes tentatively correlated to paleomagnetic reversal stratigraphy.

Table 6. Radiolarian biostratigraphic events identified in Leg 127 sediments.

Event	Species	Age (Ma)	References
FAD	*Lycnocanium* sp. cf. *L. grande*		
LAD	*Clathrocyclas cabrilloensis*		
LAD	*Sphaeropyle robusta**		
LAD	*Druppatractus acquilonius*		
LAD	*Lipmanella* sp. aff. *Theocyrtis redondoensis*		
FAD	*Theocalyptra davisiana**	2.5–2.6	(1)
LAD	*Thecosphaera japonica*		
FAD	*Sphaeropyle langii**		
LAD	*Stylacontarium* sp. cf. *S. acquilonarium*		
FAD	*Druppatractus acquilonius*		
LAD	*Thecosphaera akitoensis*		
FAD	*Thecosphaera akitoensis*		
FAD	*Lipmanella* sp. aff. *Theocyrtis redondoensis*		
LAD	*Botryostrobus bramlettei*	4.1–5.0	(2)
LAD	*Stichocorys peregrina*	2.5–2.9	(2)
LAD	*Theocyrtis redondoensis*		
LAD	*Sethocyrtis japonica*		
FAD	*Thecosphaera japonica**		
LAD	*Lychnocanium nipponicum*		
LAD	*Stichocorys delmontensis*	5.9–6.7	(2)
LAD	*Tholospyris anthopora**		
LAD	*Tholospyris mammillaris*		
LAD	*Stichocorys wolfii*	8.0–8.2	(2)
LAD	*Lithotractus tochigiensis*		
LAD	*Cyrtocapsella tetrapera*	11.6–12.1	(2)

*Zonally diagnostic species
LAD = Last appearance datum level
FAD = First appearance datum level
(1) Alexandrovich and Hays (unpublished data)
(2) Johnson and Nigrini (1985)

To apply zonations to Leg 127 sediments, the existing zonal schemes were modified to accommodate the radiolarian assemblages encountered. All radiolarian biostratigraphic events identified in sediments recovered during Leg 127 were identified with strict morphological definitions and are listed in Table 6. Miocene and early Pliocene zones are after Nakaseko and Sugano (1973) and have been amended as follows:

Cyrtocapsella tetrapera Zone. The base of this zone was not encountered during Leg 127, so its definition has not been modified and is determined by the FAD of *Hexacontium nadauraense* and *Lithopera renzae*. The top of this zone is defined by the LAD of *Tholospyris anthopora*, which agrees with the ranges and zonal boundaries in Nakaseko and Sugano (1973, Fig. 3). This definition differs from that of Nakaseko and Sugano (1973), who identify the top of this zone by the abrupt decreases in abundance of *Cyrtocapsella tetrapera* and *Lithatractus tochigiensis*. This zone is late Miocene in age.

Lychnocanium nipponicum Zone. The base of this zone is defined by the top of the *Cyrtocapsella tetrapera* Zone (LAD of *Tholospyris anthopora*), and the top is defined by the FAD of *Theocyrtis japonica* as stated by Nakaseko and Sugano (1973). *Lychnocanium nipponicum* ranges through this zone, and its

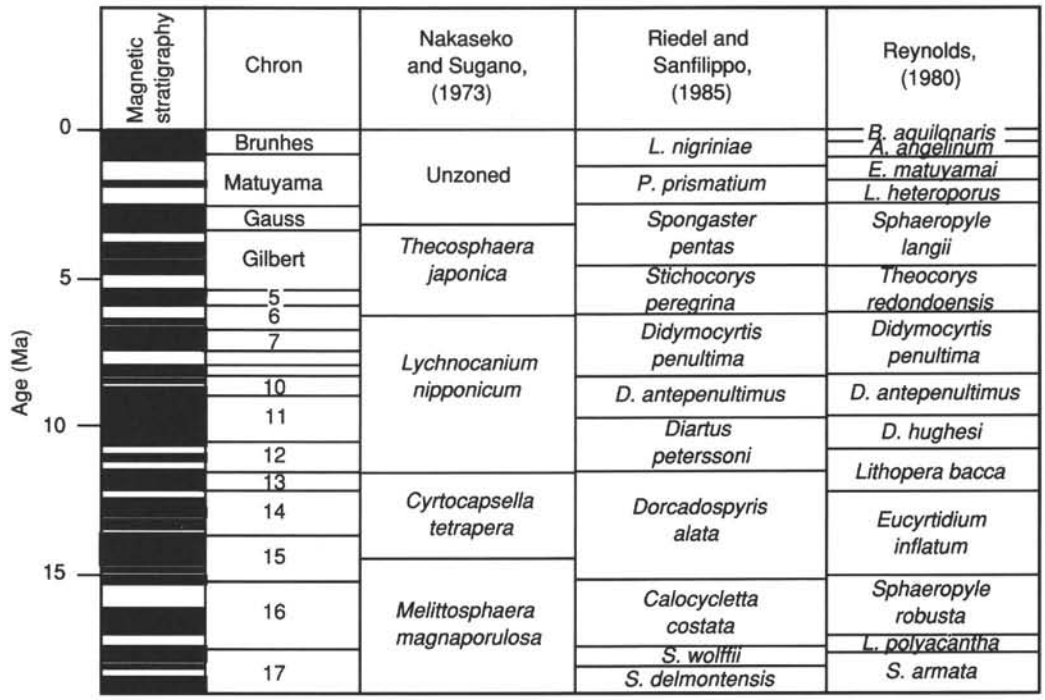

Figure 9. Correlation of Japan Sea, tropical Pacific, and North Pacific radiolarian zonations. After Nakaseko and Sugano (1973), Sanfilippo et al. (1985), and Reynolds (1980).

LAD is coincident with the top of this zone in Leg 127 sediments. This zone is late Miocene in age.

Thecosphaera japonica Zone. The base of this zone is defined by the top of the *Lychnocanium nipponicum* Zone (FAD of *Thecosphaera japonica*). This differs from Nakaseko and Sugano (1973) by not including the FAD of *Spongurus inouei* as a basal indicator. The top of this zone was not defined by Nakaseko and Sugano (1973) because preserved radiolarians have not been found in upper Pliocene and Quaternary marine sediments of Japan. Therefore, it was necessary to amend the zonation of Nakaseko and Sugano (1973) to accommodate the upper Pliocene and Quaternary sediments recovered during Leg 127. The top of this zone is defined by the FAD of *Sphaeropyle langii*. This zone ranges from late Miocene to Pliocene in age and is correlative with the *Theocyrtis redondoensis* Zone of Reynolds (1980). The transition of *Druppatractis lacquilonius (Stylacontarium acquilonarium*) from *S.* sp. cf. *S. acquilonarium* occurs near the top of this zone instead of in the *Sphaeropyle langii* Zone as reported by Reynolds (1980).

The following three zones are tentative and designed to utilize the radiolarian species found in upper Pliocene and Pleistocene Leg 127 sediments. All of the datum levels used to define these zones are discussed in Reynolds (1980), and allow tentative correlations between those zonations and the zonations presented here.

Sphaeropyle langii Zone. The base of this zone is defined by the FAD of *Sphaeropyle langii* and is consistent with the definition as originally proposed by Foreman (1975) and outlined by Reynolds (1980). The top of this zone is changed, however, and defined by the base of the *Sphaeropyle robusta* Zone (FAD of *Theocalyptra davisiana*). This zone correlates to the *Sphaeropyle langii* and lower *Lamprocyrtis heteroporus* Zones as outlined in Reynolds (1980) and is late Pliocene in age.

Sphaeropyle robusta Zone. The base of this zone is defined by the FAD of *Theocalyptra davisiana*. The top is defined by the base of the *Theocalyptra davisiana* Zone (LAD of *Sphaeropyle robusta*). The FAD of *Theocalyptra* davisiana has been dated in tropical Pacific cores at 2.49–2.59 Ma. (Alexandrovich and Hays, unpubl. data), and the event appears to be synchronous in the Japan Sea. The *Sphaeropyle robusta* Zone correlates to the upper half of the *Lamprocyrtis heteroporus* Zone outlined in Reynolds (1980) and is late Pliocene to Pleistocene in age.

Theocalyptra davisiana Zone. The base of this zone is defined by the LAD of *Sphaeropyle robusta*. The top of this zone extends into Holocene sediments. This zone is correlative with the *Botryostrobus aquilonaris, Axoprunum angelium*, and most of the *Eucyrtidium matuyamai* Zones as summarized in Reynolds (1980). The zone is Quaternary in age.

Sample Preparation and Examination

Radiolarians were extracted from core-catcher samples and mounted on slides for microscopic examination using standard methods described by Sanfilippo et al. (1985). Sediment samples of approximately 5 cm^3 were disaggregated and oxidized in 10% hydrogen peroxide solution. When calcium carbonate was present, 10% hydrochloric acid was added to dissolve the calcareous components. Samples were further disaggregated by adding 1% Calgon solution to deflocculate the clays. The samples were treated to brief ultrasonification, then washed in a 63-μm sieve several times to remove the clays. The resulting residues were composed of radiolarians, medium silt, large centric diatoms (*Coscinodiscus marginatus*) and diatom girdles. These residues suspended in distilled water were pipetted (strewn) evenly onto labeled glass slides and the excess water was evaporated on a hot plate. Finally, a 22- by 50-mm cover slip was mounted to the slide with Canada Balsam. Two slides were prepared and examined for each sample. The wet residue was retained in the event that re-examination of the material proved necessary.

The preservation and abundance of the radiolarian assemblages were assessed semi-quantitatively in each core-catcher sample. As samples were not weighed, the relative abundance of

radiolarians in each sample was based on an estimation of the number of radiolarians per cubic centimeter of the original sample. Radiolarian assemblage abundance was assessed as follows:

A = Abundant, 10^4 radiolarians per cm^3.
C = Common, 10^3 radiolarians per cm^3.
F = Few, 10^2 radiolarians per cm^3.
R = Rare, 10 radiolarians per cm^3.
B = Barren, no radiolarians found in the sample.

Preservation of the radiolarian assemblages was determined as follows:

Good: Radiolarian assemblages that contain individuals showing little or no fragmentation, intact spines, and normal indices of refraction.

Moderate: Radiolarian assemblages where specimens show frequent fragmentation and/or high indexes of refraction.

Poor: Radiolarian assemblages that are composed mainly of broken specimens and individuals that show signs of dissolution (no preserved delicate lattice components or visible solution features).

Relative abundances of diagnostic taxa (species abundances) were determined semiquantitatively as follows:

A = Abundant, >10% of the total radiolarian assemblage.
C = Common, 1%–10% of the total radiolarian assemblage.
F = Few, 0.1%–1% of the total radiolarian assemblage.
R = Rare, 0.01%–0.1% of the total radiolarian assemblage.
B = Barren, <0.01% of the total radiolarian assemblage.

PALEOMAGNETISM

Natural remanent magnetization (NRM) and magnetic susceptibility (K) measurements are routinely performed on board the *JOIDES Resolution*. Because most of the rocks have been affected by secondary magnetizations, magnetic cleaning by alternating field (AF) or thermal demagnetizations were necessary to obtain the characteristic remanent magnetization (ChRM) of the rock. At Site 797, the isothermal magnetization (IRM) acquired in a field of 500 mT was studied to get some quantitative and qualitative information of the carrier of the ferrimagnetic properties.

Instruments

Three magnetometers, two Molspin spinner magnetometers and a 2-G Enterprises (model 760R) pass-through cryogenic superconducting rock magnetometer, were available for measurement of remanence on board the *JOIDES Resolution* during Leg 127. An AF demagnetizer (Model 2G600) capable of alternating fields up to 25 mT is on-line with the cryogenic magnetometer. Both are controlled by a FASTCOM4 multiserial communication board in an IBM PC-AT compatible computer. The measurements were performed by the paleomagnetists using Quickbase program MAG 127, a slightly modified version of the MAG program used on Leg 126. The spinner magnetometer is controlled by a Digital PRO350 computer and is used only to measure individual samples. For NRM measurements the program MINISPIN.OAS (written by Y. Hamano, Leg 109, and modified during Leg 124) was used. To speed up the IRM measurements, J. Wippern (Leg 127) modified this program. The new version (IRM 127.BAS) calculates declination, inclination, and intensity, measuring the first two positions required by the original program.

The superconducting quantum interference device (SQUID) sensors in the cryogenic magnetometer measure magnetization over an interval approximately 20 cm long. Each axis has a slightly different response curve. The widths of the sensor regions imply that as much as 150 cm^3 of core contributes to the sensor signals. The large volume of core material within the sensor region permits an accurate determination of remanence for weakly magnetized samples despite the relatively high background noise related to the motion of the ship. The SQUID electronics operate at the 1X scale for sediments and at 100X scale for basaltic rocks. If sediments and basaltic rocks occur in the same section, the measurements of the weaker sediments are hampered by this procedure and it is necessary to measure the two lithologies separately.

APC cores were oriented with respect to north by the multishot orientation tool. The paleomagnetic results were then correlated for the orientation of the core. However, except at Site 794, the directions were calculated and plotted in the core coordinates.

Remanent Magnetization Measurements

The maximum AF demagnetizing field allowed for sections from the archive half is 15 mT or the median destructive field, whichever is lower. Discrete samples from the working half of the core may also be AF demagnetized using the Schonstedt GSD-1 (max peak field 99 mT).

Sediments

Remanence measurements of sediments were performed by passing continuous archive-half core sections through the cryogenic magnetometer. NRM measurements were taken at 10-cm intervals along the cores before and after AF demagnetization in two steps generally of 8–10 and 15 mT. Sometimes a further step with a lower peak-field of 4 mT was used for very weak sediments. Discrete samples were taken from APC, XCB, and RCB sediment cores by pressing a standard plastic sampling box (7 cm^3) into the soft-core material. The uphole direction was marked on the box. For more consolidated sediments, a spatula was used to cut the cubes. Up to three discrete samples per section were collected from working cores to check the results from the whole-core measurements.

Basement Rocks

The NRM of the basaltic rock recovered from dikes, sills, and volcanic flows was generally too strong to be measured with the cryogenic magnetometer. However, after AF cleaning with 8–10 mT, the intensity decreased to a value acceptable for this magnetometer. Minicores were drilled from the basaltic rocks and were measured with the Molspin magnetometer to check higher coercivity components.

Isothermal Remanent Magnetization (IRM)

At Site 797, samples destined for a shore-based paleontological study (1 per section, mostly at the the same interval) were collected using paleomagnetic cubes. The samples were magnetized along the Z-axis with a field of 500 mT using the pulse magnetometer available on the *JOIDES Resolution*. The acquired IRM was AF-demagnetized parallel to the Z-axis in three steps (5, 15, and 55 mT). Sometimes we used additional steps of 35 and 85 mT to obtain more detailed observations of the coercivity spectrum. Because the ODP naming scheme is not very flexible, we labeled these rock magnetic measurements with 500 A, 505 A, and 515 A and so on.

Magnetic Stratigraphy

In agreement with the paleontologists, the magnetostratigraphic time scale of Berggren et al. (1985) was adopted for use during the leg.

Magnetic Susceptibility Measurements

Magnetic susceptibility measurements were routinely made on all cores employing a Bartington Instrument magnetic susceptibility meter (model M.S.1) with a M.S.1/CX, 80-mm whole-core sensor loop set at 0.47 kHz (range 1). The susceptibility meter is on-line with the gamma-ray attenuation porosity evaluator (GRAPE) and *P*-wave logger on the multisensor track (MST). The general trend in the susceptibility data was used to characterize the cored sediments. Igneous rock susceptibility was used to calculate the induced magnetization assuming a local magnetic field value of 46,000 nanotesla (nT).

INORGANIC GEOCHEMISTRY

The shipboard analytical program for inorganic geochemistry focused solely on the chemical characterization of interstitial waters extracted from 5 cm-long whole-round sediment samples. On Leg 127, interstitial waters were obtained both by squeezing with the standard ODP stainless-steel squeezer (Manheim and Sayles, 1974) and with a plastic-lined squeezer (Brumsack et al., in preparation) designed specially for obtaining uncontaminated interstitial water samples for shore-based trace metal analysis. At each site, 5-cm samples for the ODP squeezer were taken from the first and third core, and from every third core thereafter, when recovery was sufficient. Samples for the plastic squeezer were taken from the first ten sediment cores and then every third core thereafter. Wherever possible, the ODP samples and the plastic squeezer samples were taken adjacent to each other. At Sites 795 and 797, additional samples were taken near and across the opal-A/opal-CT silica phase transformation. The locations of the routine ODP interstitial water samples (IW) and the additional plastic-squeezed sample, termed Brumsack/Murray (BM), are noted on the summary core description forms for each site.

The whole-round sections were immediately cut from the core when it arrived on deck and capped at both ends. Each IW sample was removed from the core liner, scraped with a spatula to remove the potentially contaminated exterior of the sample, placed into the standard ODP stainless-steel squeezer, and pressed in a Carver hydraulic press at pressures up to 40,000 psi. The extracted IW samples were collected directly into a 50-mL plastic syringe and filtered through an on-line 0.45-μm Gelman Acrodisc disposable filter. In contrast to the routine shipboard procedure, the capped BM core sections were immediately placed in a nitrogen-filled glove bag to prevent oxidation. While in the nitrogen bag, they were removed from the core liner, scraped with a plastic spatula, and loaded into the plastic-lined squeezer. They were squeezed at pressures up to 20,000 psi in the Carver press. The BM samples were ejected through a 0.45-μm Millipore polycarbonate membrane filter placed inside the squeezer and so were not passed through the syringe/filter apparatus described above. The BM samples were collected in pre-cleaned plastic vials for transport to the shore-based laboratories.

IW waters were routinely analyzed for alkalinity, pH, salinity, chlorinity, silica, phosphate, ammonium, sulfate, calcium, and magnesium, following the analytical techniques described in Gieskes and Peretsman (1986). Where sample volume were large, BM waters were also analyzed for some of these major chemical constituents, allowing comparison between IW- and BM-squeezing techniques and apparatus.

Lithium, sodium, rubidium, and potassium were determined on the shipboard atomic absorption spectrophotometer in the emission mode (AES) after adequate dilution and addition of either an ionization buffer (Suprapure CsCl) or an appropriate matrix modification, and calibrated against synthetic seawater standards. Details of the methods have been developed in the laboratory of one of the shipboard inorganic geochemists (Brumsack). Strontium was analyzed by conventional atomic absorption spectrophotometry (AAS).

ORGANIC GEOCHEMISTRY

Shipboard organic geochemistry during Leg 127 of the ODP was conducted to supply a real-time monitoring of the volatile hydrocarbons for safety considerations and for an initial characterization of the content and type of organic matter in the sediments. These analyses provide a basis for the preliminary site summaries and background for more detailed shore-based studies that will follow. The characterization of the sources and preservation of organic matter in sediments of the Japan Sea is necessary to delineate its paleoceanographic history and fulfill the overall objectives of the Leg 127 (Japan Sea I) drilling program (see Introduction, this volume).

Hydrocarbon Gases

As required by safety considerations, the concentrations of the hydrocarbons methane (C1), ethane (C2), and propane (C3) were monitored in the sediment cores at intervals of about 10 m. The hydrocarbon gases were extracted from bulk sediment using a headspace-sampling technique. A 5-cm^3 plug of sediment was taken as the core arrived on deck, using a No. 4 cork borer. The sample was placed immediately in a glass vial that was sealed with a septum and metal crimp and then heated to 70°C. The gas driven off was drawn into a syringe and injected into a Hach-Carle AGC Series 100 model 211 gas chromatograph equipped with a thermal conductivity detector and a 6-ft × ⅛-in. steel column packed with Porapak N:Q (80%/20%). Where high concentrations of propane were suspected, a second sample was taken using the same method and analyzed for C1 through C6 hydrocarbons using a Hewlett-Packard 5980A Natural Gas Analyzer, a gas chromatograph equipped with a 6-in. × ⅛-in. steel column packed with Poropak T, a 3-ft × ⅛-in. steel column packed with 13X molecular-sieve, a 6-ft × ⅛-in. steel column packed with 80/100 mesh Hayesep R(AW), and a DB1 (1-μm film thickness, J&W) fused silica capillary column (60-m × 0.32-mm i.d.). Compounds were detected using both a thermal conductivity and a flame ionization detector. Details of this method and the complete configuration of both gas chromatographs are given in the Leg 112 Explanatory Notes (Shipboard Scientific Party, 1988a).

Elemental Analysis

Sediments were analyzed on board ship for inorganic carbon and for total nitrogen, carbon, and sulfur. The organic carbon content of the sediments was then calculated by difference. Inorganic carbon and total nitrogen, carbon and occasionally sulfur were determined on most of the sediment samples taken for physical-properties measurements and headspace analysis and on subsamples of the squeeze-cake generated during interstitial water isolation. All samples were freeze-dried prior to analysis.

Total inorganic carbon was determined using a Coulometrics 5011 Coulometer equipped with a System 140 carbonate carbon analyzer. Depending on carbonate content, 15 to 70 mg of ground and weighed sediment was reacted in a 2N HCl solution. The liberated CO_2 was titrated in a monoethanolamine solution with a colorimetric indicator, while the change in light transmittance was monitored with a photo-detection cell.

Total nitrogen, carbon, and sulfur were determined using a N/C/S analyzer, model NA 1500 from Carlo Erba Instruments. Bulk samples were combusted at 1000°C in an oxygen atmosphere with addition of vanadium pentoxide, converting organic and inorganic carbon to CO_2 and sulfur to SO_2. These gases along with nitrogen were then separated by gas chromatography and measured with a thermal conductivity detector.

Rock-Eval Analysis

Organic matter type, thermal maturity, and hydrocarbon producing potential were assessed using a Delsi Inc. Rock-Eval II

Plus total organic carbon instrument. Approximately 100 mg of freeze-dried and ground whole sediments were analyzed according to standard procedures as described in Emeis and Kvenvolden (1986) and references therein. Additional guidelines for interpretation of results and discussion thereof can be found in Katz (1983) and Peters (1986).

BASEMENT ROCKS

Core Curation and Shipboard Sampling

To preserve important features and structures, core sections containing basement rocks were examined prior to splitting with a diamond saw into archive and working halves. During core handling and splitting, care was taken to ensure that the core orientation was preserved by marking the original base of individual pieces. Each piece was numbered sequentially from the top of each core section and labeled at the top surface. Pieces that could fit together were assigned the same number, but were lettered consecutively (e.g., 1A, 1B, and 1C). Plastic spacers were placed only between pieces with different numbers. The presence of a spacer, therefore, may represent a substantial interval of no recovery. If it could be determined that individual pieces did not rotate about a horizontal axis during drilling, an arrow was added to the label pointing to the top of the section. As pieces were free to turn about a vertical axis during drilling, azimuthal orientation was not possible.

After the core was split, the working half was sampled for shipboard physical properties, magnetic studies, X-ray fluorescence, X-ray diffraction, and thin section studies. Non-destructive physical property measurements, such as magnetic susceptibility, were made on the archive half of the core. Where recovery permitted, samples were taken from each lithologic unit. Some of these samples were minicores. The archive half was described on the visual core description form and was photographed before storage.

Visual Core Descriptions

Visual core descriptions were used in the basement cores (see site summary appendices). The left column is a graphic representation of the archive half. A horizontal line across the entire width of the column denotes a plastic spacer. Oriented pieces are indicated on the form by an upward-pointing arrow to the right of the piece. Shipboard samples and studies are indicated in the column headed "shipboard studies" using the following notation: XD = X-ray diffraction analysis; XF = X-ray fluorescence analysis; TB = petrographic thin section; PP = physical properties analysis; and PM = paleomagnetic analysis.

To ensure consistent and complete descriptions, the visual core descriptions were entered into the computerized database HARVI. This database is organized into records for fine-grained rocks and records for coarse-grained rocks. Each record is checked by the data-base program for consistency and is printed in a format that can be directly pasted onto the barrel sheet for subsequent curatorial handling.

When describing sequences of rocks, the core was subdivided into lithologic units, using changes in petrography, mineral abundance, rock composition, and rock clast type. For each lithologic unit and section, the following information was recorded in the data-base system:

A. The leg, site, hole, core number, core type, and section number.

B. The unit number (consecutive downhole), position in the section, number of pieces of the same lithologic type, identification of the describer, and the rock name.

C. The dry Munsell color of the rock and the presence and character of layering and deformation.

D. The number of mineral phases visible with a hand lens and their distribution within the unit. For each mineral phase, we have noted: (1) abundance (volume %); (2) size range in millimeters; (3) shape; (4) degree of alteration; and (5) further comments.

E. The groundmass texture, including the presence of glass, the nature of crystallinity, and the grain-size. For the grain-size, fine is <1 mm, medium is 1–5 mm, and coarse is >5 mm. Relative grain-size changes within the unit were also noted.

F. The presence and characteristics of secondary minerals and alteration.

G. The abundance, distribution, size, shape, and infilling material of vesicles (including the proportion of vesicles that are filled by alteration or secondary minerals).

H. The structure, including noting any internal layering and whether the flow is massive, pillowed, thin or sheetlike, brecciated, or a hyaloclastite.

I. The relative amount of rock alteration: $<2\%$, fresh; 2–10%, slightly altered; 10–40%, moderately altered; 40–80%, highly altered; 80–95%, very highly altered; and 95–100%, completely altered. The type, form, and distribution of alteration was also noted.

J. The presence of veins and fractures, including their abundance, width, and orientation. The relationship of the veins and fractures to the alteration and fillings was also noted.

K. Other comments, including notes on the continuity of the unit within the core and on the interrelationship of units.

Basalts and dolerites (diabase) were termed aphyric ($<1\%$), sparsely phyric (1–2%), moderately phyric (2–10%), or highly phyric ($>10\%$), depending upon the proportion of phenocrysts visible with the hand lens or binocular microscope. Basalts were further classified by phenocryst (e.g., a moderately plagioclase-olivine phyric basalt contains 2%–10% phenocrysts, mostly plagioclase, with subordinate olivine). Volcanic rock names were initially assigned from megascopic phenocryst assemblages. Where chemical analyses or thin-sections became available, more specific rock names were given.

Igneous and metamorphic visual core descriptions are given in the site summary appendixes, and descriptions of each rock unit are available from the computerized data base at the ODP repositories.

Thin-Section Descriptions

Thin-sections of basement rocks were examined to complement and refine the hand-specimen observations. The percentages and textural descriptions of individual phases were reported in the computerized data base HRTHIN. The terminology used for thin-section description was used in the same manner as in the megascopic descriptions. Thin-section descriptions are included in the site summary appendixes and are also available from the ODP computerized data base.

The rock description terms for basalts used in this report differ slightly from those used on previous ODP legs. Lavas erupted on the seafloor typically show a sparsely crystalline glassy margin, followed by a spherulithic zone of quench phases, which may then evolve into a coarser microlitic zone toward the interior of the flow. Spherules commonly show a sheaf-like or radial form and the microlitic zone is characterized by clustering (bowtie or radial) of microlites. Following Natland (1978, 1980) we emphasize that these textures are quench-growth features and do not represent post-solidification phenomena. We also emphasize that the term microlitic texture is independent of whether phenocrysts are present or not. Finally, we use the term intergranular to refer to groundmass textures where the individual crystals of minerals other than plagioclase are granule-shaped with little intergrowth.

X-ray Diffraction Analyses

A Philips ADP 3520 X-ray diffraction was used for the X-ray diffraction (XRD) analysis of mineral phases. CuK-alpha radiation was measured through a Ni filter at 40 kV and 35 Ma. The goniometer scanned from 2° to 70° 2Θ with a step size of 0.02°, and the counting time was 1 s per step.

Samples were ground in a Spex 8000 Mixer Mill or an agate mortar with pestle. The powder was then pressed into the sample holders or smeared on glass plates for analysis. Diffractograms were interpreted with the help of a computerized search and match routine using the Joint Committee on Powder Diffraction Standards powder files.

X-ray Fluorescence Analysis

Prior to analysis, samples were normally crushed in the Spex 8510 shatterbox using a tungsten carbide barrel. This produces some Ta and massive W contamination, resulting in the powder becoming unsuitable for instrumental neutron activation (INNA) analysis.

A fully automated wavelength-dispersive ARL8420 XRF (3 kW) system equipped with an Rh target X-ray tube was used to determine the major oxide and trace-element abundances of whole rock samples. Analyses of the major oxides were carried out on lithium borate glass disks doped with lanthanum as a "heavy absorber" (Norrish and Hutton, 1969). The disk were prepared from 500 mg of rock powder, ignited for 2 hr at about 1030°C, and mixed with 6.000 g of dry flux consisting of 80% lithium tetraborate and 20% La_2O_3. This mixture was then melted in air at 1150°C in a Pt-Au crucible for about 10 min and poured into a Pt-Au mold using a Claisse fluxer. The 12:1 flux-to-sample ratio and the use of the lanthanum absorber made matrix effects insignificant over the normal range of igneous rock compositions. Hence the relationship between X-ray intensity and concentration becomes linear and can be described by:

$$C_i = (I_i \cdot m_i) - b_i$$

where C_i = concentration of oxide i (wt.%); I_i = net peak X-ray intensity of oxide i; m_i = slope curve for oxide i (wt%/cps); and b_i = apparent background concentration for oxide i (wt.%)

The slope m_i was calculated from a calibration curve derived from the measurement of well-analyzed reference rocks (BHVO-1, G-2, AGV-1, JGB-1, JP-1, BR, and DRN). The background b_i was determined either on blanks or derived by regression analysis from the calibration curves.

Systematic errors resulting from short-term or long-term fluctuations in X-ray tube intensity were corrected by normalizing the measured intensities of the samples to those of a standard that was always run together with a set of six samples. To reduce shipboard weighing errors, two glass disks were prepared for each sample. Accurate weighing was difficult on board the moving platform of the *JOIDES Resolution*, and was performed with particular care as weighing errors could be a major source of imprecision in the final analysis. Loss-on-ignition values were determined by drying the sample at 110°C for 8 hr, and then by weighing before and after ignition at 1030°C in air.

Trace-element determinations were made on pressed-powder pellets by pressing (with 7 tons of pressure) a mixture of 5.0 g of dry-rock powder (dried at 110°C for >2 hr) and 30 drops of polyvinyl alcohol binder into an aluminum cap. A modified Compton scattering technique based on the intensity of the Rh Compton peak was used for matrix absorption corrections (Reynolds, 1967).

Replicate analyses of rock standards show that the major-element data are precise to within 0.5 to 2.5% and are considered accurate to ±1% for Si, Ti, Fe, Ca, and K, and to ±3–5% for Al, Mn, Na, and P. The trace-element data are considered accurate to ±2–3% or 1 ppm (whichever is greater) for Rb, Sr, Y, and Zr, and ±5–10% or 1 ppm for the others, except for Ba and Ce. Precision is also within 3% for Ni, Cr, and V at concentrations >100 ppm. The range of trace-element concentrations over which these claims hold encompasses those encountered during Leg 127. Analytical conditions for the XRF analyses are given in Table 7.

PHYSICAL PROPERTIES

The shipboard measurement of physical properties provides information that can aid in the characterization of different lithologic units, allows a verification of the downhole geophysical logging results, and provides important constraints on the interpretation of seismic reflection and other geophysical data. Furthermore, these data may be used to estimate the degree of consolidation, correct sedimentation rates, aid in heat-flow calculations, and provide additional data for paleoceanographic interpretation of the cores. Depth profiles of the geotechnical properties may be used for distinguishing lithologic boundaries at drill sites as well as for correlating and establishing facies changes between sites.

Physical property measurements made on cores recovered during Leg 127 included: multi-sensor-track (MST) logging of gamma-ray attenuation porosity evaluator (GRAPE) bulk density, compressional acoustic velocity measurements and magnetic susceptibility; thermal conductivity; Hamilton Frame compressional velocity; electrical resistivity; index properties; grain-size analyses; and carbonate content analyses. Samples were chosen to be representative of the core or section as a whole, and were taken in areas of least disturbance. Sample selection and spacing depended on the core recovery, the type of measurement (see below), and the thickness and homogeneity of the recovered sequences.

We note that shear-vane measurements of undrained shear strength were not taken on Leg 127. The shear vane is designed for use with clayey sediments having shear strengths less than 100 kPa (Craig, 1983), and results for sediments with any significant non-clay component and/or shear strength are not valid. In addition, the undrained shear strength cannot be readily related to other strength properties. We therefore decided to omit the vane shear tests from the Leg 127 physical properties program.

The testing methods employed during Leg 127 are discussed in the order in which they were performed on each core. MST logging and soft sediment thermal conductivity determinations were performed first on whole cores still within their liners. All other measurements were conducted on discrete samples taken from the split cores.

Gamma-ray Attenuation Porosity Evaluator (GRAPE)

The gamma-ray attenuation porosity evaluator (GRAPE) makes continuous measurements of wet-bulk density on whole cores by comparing attenuation of gamma rays through the cores with attenuation through an aluminum standard (Boyce, 1976). Individual core sections were placed horizontally on the multi-sensor track (MST), and moved on a conveyor belt through the GRAPE sensors. The attenuation of the gamma rays passing through the liner and core is measured every 1 cm, and the bulk density is calculated from the attenuation values. The raw GRAPE data were not filtered or averaged. All bulk density data are reported in units of g/cm^3. Because of grain-density variations, porosity cannot be reliably determined from the GRAPE density measurements, and because of variable drilling disturbance downcore the absolute density values should be used for qualitative purposes only. The GRAPE is best used to show relative, rather than absolute, density changes along the core for correla-

Table 7. Leg 127 X-ray fluorescence analytical conditions.

Element	Line	Crystal	Detector	Collimator	Peak angle (deg.)	Background offset (deg.)	Total count time (seconds)	
							Peak	Background
SiO_2	Kα	PET(002)	FPC	Coarse	109.25	0	40	0
TiO_2	Kα	LIF(200)	FPC	Fine	86.14	0	40	0
Al_2O_3	Kα	PET(002)	FPC	Coarse	145.27	0	100	0
Fe_2O_3	Kα	LiF(200)	FPC	Fine	57.52	0	40	0
MnO	Kα	LiF(200)	KrSC	Fine	62.98	0	40	0
MgO	Kα	TLAP	FPC	Coarse	44.87	±0.80	200	200
CaO	Kα	LiF(200)	FPC	Coarse	113.16	0	40	0
Na_2O	Kα	TLAP	FPC	Coarse	54.71	−1.20	200	200
K_2O	Kα	LiF(200)	FPC	Fine	136.65	0	40	0
P_2O_5	Kα	Ge(111)	FPC	Coarse	140.94	0	100	0
Rh	K-C	LiF(200)	Scint.	Fine	18.59	0	100	0
Nb	Kα	LiF(200)	Scint.	Fine	21.37	±0.35	200	200
Zr	Kα	LiF(200)	Scint.	Fine	22.53	±0.35	100	100
Y	Kα	LiF(200)	Scint.	Fine	23.78	±0.40	100	100
Sr	Kα	LiF(200)	Scint.	Fine	25.13	±0.40	100	100
Rb	Kα	LiF(200)	Scint.	Fine	26.60	±0.60	100	100
Zn	Kα	LiF(200)	Scint.	Fine	41.79	±0.40	60	60
Cu	Kα	LiF(200)	Scint.	Fine	45.02	±0.40	60	60
Ni	Kα	LiF(200)	Scint.	Coarse	48.67	±0.60	60	60
Cr	Kα	LiF(200)	FPC	Fine	69.35	±0.50	60	60
Fe	Kα	LiF(220)	FPC	Fine	85.37	−0.40 + 0.70	40	40
V	Kα	LiF(220)	FPC	Fine	122.84	−0.50	60	60
TiO_2	Kα	LiF(200)	FPC	Fine	86.14	±0.50	40	40
Ce	Lα	LiF(220)	FPC	Coarse	127.92	±1.50	100	100
Ba	Lβ	LiF(220)	FPC	Coarse	128.53	±1.50	100	100

* Total Fe as Fe_2O_3
** Calibrated, but not analyzed on basalts
FPC: Flow proportional counter using P_{10} gas
KrSC: Sealed Krypton gas counter
Scint.: NaI scintillation counter
All elements analyzed under vacuum on gonimeter 1, at generator settings of 60 kV and 50 mA.

tion with lithologic changes (Shipboard Scientific Party, 1988b). GRAPE data are used to correlate between holes and sites by observing peak-to-peak spacings and general trends in the data.

P-Wave Logger (PWL)

The *P*-wave Logger (PWL), which also operates on the MST, transmits a 50-kHz compressional-wave pulse through the core at a repetition rate of 1 kHz. The transmitting and receiving transducers are aligned perpendicular to the core axis. A pair of displacement transducers monitor the separation between the compressional-wave transducers; variations in the outside liner diameter therefore do not degrade the accuracy of the velocities. Measurements are taken at 2-cm intervals. Keeping the core liner wet during the PWL run improves acoustic contact between the transducers and the liner.

As with the GRAPE, generally only APC and the first few XCB cores were measured. The deeper XCB cores and all RCB cores have annular voids between the core and the liner, which causes transmission losses. The PWL data were filtered to remove data resulting from gas, or gaps, or end-gap effects. Weak returns with signal strengths below a threshold value of 100 were removed. All velocity data are reported in units of m/s. As with the GRAPE data, PWL data are used to correlate between holes and sites.

Magnetic Susceptibility

MST magnetic susceptibility measurements were routinely made on all cores at 10-cm intervals by employing a Bartington Instrument magnetic susceptibility meter (model M.S.1) with a M.S.1/CX 80-mm whole-core sensor loop set at 0.47 kHz. The magnetic susceptibility values are recorded in cgs units. In addition to characterizing the cored sediments, susceptibility data are used to correlate between holes and sites.

Thermal Conductivity

The thermal conductivity measurements techniques used are described by von Herzen and Maxwell (1959) and Vacquier (1985). All thermal conductivity data are reported in units of W/m K, the standard SI unit. The error in the reported measurements was estimated to be about 5%.

Soft Sediment Thermal Conductivity

Measurements are made with a Thermcon-85 unit. To reduce background thermal transients, cores were allowed to equilibrate to room temperature in their liners for at least 3 hr. One needle probe per section, on average, was inserted into the sediment through holes drilled through the core liner. After a brief wait for temperatures to stabilize, the probe heaters were turned on at a constant power, and the temperature rise of the probe was recorded. Thermal conductivity is calculated from a 4- to 6-min temperature history after the heaters are energized.

After the heater has been on for about 30 s, the needle probe response is very close to that of a line source with a constant heat generation per unit length. The temperature rise varies logarithmically with time as:

$$T(t) = (q/4\pi K)\ln(t) + \text{const.} \quad (1)$$

where k is the thermal conductivity, T and t are the temperature and time, respectively, and q is the heat generated per unit length of the probe in J/m. From (1), the thermal conductivity is derived from the slope of temperature vs. the logarithm of time:

$$k = (q/4\pi)/(dT/dln(t)) \quad (2)$$

When the sediment became too firm to allow easy insertion of the probe, holes were drilled into the core material prior to

insertion. We attempted to insert the probes at locations where the core section appeared to be least disturbed. However, an annulus of disturbed sediment and drill fluid was often present along the inside of the liner, preventing visual identification of disturbed zones; consequently, spurious values associated with voids are possible.

Needle Probe Calibration

Several conductivity needle probes were fabricated on board for this leg to augment the few working probes that were left from previous legs. Calibrations of temperature vs. resistance were made for all of the probes currently on the ship. A Lauda temperature bath and a Fluke digital multimeter were used to make the calibrations over the range from 20° to 50°C. The calibration data are fitted to an equation of the form:

$$T = 1/(A + B \cdot \ln(R) + C \cdot \ln(R)^3) \quad (3)$$

where T is the temperature in kelvin and R is the resistance in ohms. The calibration data fit (3) with an average standard deviation of about 0.03 K.

Hard-Rock Thermal Conductivity

Thermal conductivity measurements on lithified sediments and rocks were conducted on split cores using the "half-space technique" (Vacquier, 1985). In this method the rock sample with one flat surface was placed on top of a needle probe that is embedded along the surface of a slab of low-conductivity material. The flat surface of the sample was polished with 240 grit to minimize pockets of water or air and thus to assure good contact with the slab containing the needle probe. A heat-conducting compound was used to improve the thermal contact between the slab and the sample. The experiment was immersed in a salt-water bath to maintain a uniform temperature, to avoid cooling by evaporation, and to keep the sample saturated with water.

The experimental procedure for the half-space method is exactly the same as for the needle probe. The probe heater was turned on, and the temperature of the probe is recorded over a 4-min interval. No simple analytical model for this experiment exists, but we know from experience that the temperature vs. time records produced by the half-space technique follow a nearly logarithmic relation like equation (1). Thus we can reduce the results of the half-space experiment as though it were a full-space needle-probe experiment (i.e., using Eq. 2) and apply an empirically determined conversion formula. The response will depend on the conductivity contrast as well as the conductivity of the sample, consequently a constant multiplicative factor can only be used over a small range of conductivities.

A conversion formula was derived by calibrating the half-space experiment vs. the needle probe method using three reference materials on the *JOIDES Resolution*. The references have conductivities that span the range of likely conductivities to be encountered in ODP samples. All of the experiments for the calibration were run for 4 min., and were reduced using the same computer program (NTRTHERM.BAS). The results of the calibration are shown in Table 8 and Figure 10. The three points of comparison are fit by a linear relation:

$$K_u = -0.180 + 2.44 \cdot K_a, \quad (4)$$

where K_u is the conductivity of the reference using the needle-probe method and K_a the apparent conductivity from the half-space experiment reduced using Equation (2). Equation (4) was used in reduction programs on Leg 127 to reduce results from the half-space conductivity measurements on hard-rock samples.

Table 8. Calibration of the half-space thermal conductivity experiment.

Reference material	Needle probe K_{avg}**	Needle probe Std. Dev.	Half-space exp. K_{avg}*
Macor ceramic	1.637	0.167	0.744
Red rubber	0.906	0.048	0.446
Black plastic	0.488	0.019	0.273

* Three measurements were averaged. The standard deviation was less than 5%.
** The average of 10 or more measurements.

Our approach to determining a conversion formula differs from that of Von Herzen on Leg 118 (see the Site 735 Summary, Robinson, Von Herzen, et al., 1989). He used two relatively high-conductivity reference materials, the Macor ceramic and Fused Silica, and conducted experiments for 6 min. The temperature histories for the half-space conductivity experiments on the *JOIDES Resolution* are not strictly linear on a T vs. ln(t) plot; he therefore selected the most linear portion of the curves, usually for times greater than 90 s to use in Equation (2). This invariably leads to lower values of $\Delta T/\Delta \ln(t)$ and higher apparent conductivities. He determined a conversion factor that was slightly less than 2.0, which is more consistent with theory. Von Herzen's approach will yield accurate measurements of conductivity, but requires the scientist interpreting the data to develop a consistent set of criteria for picking the right interval of the temperature record over which to determine the slope. This may be difficult for persons not intimately familiar with needle-probe measurements and difficult to document. Thus we preferred an approach that analyses the same interval of the temperature history and the same reduction procedure for all experiments.

Hamilton Frame Compressional-Wave Velocity

Compressional-wave velocity measurements were taken on discrete samples that were sufficiently competent to provide ade-

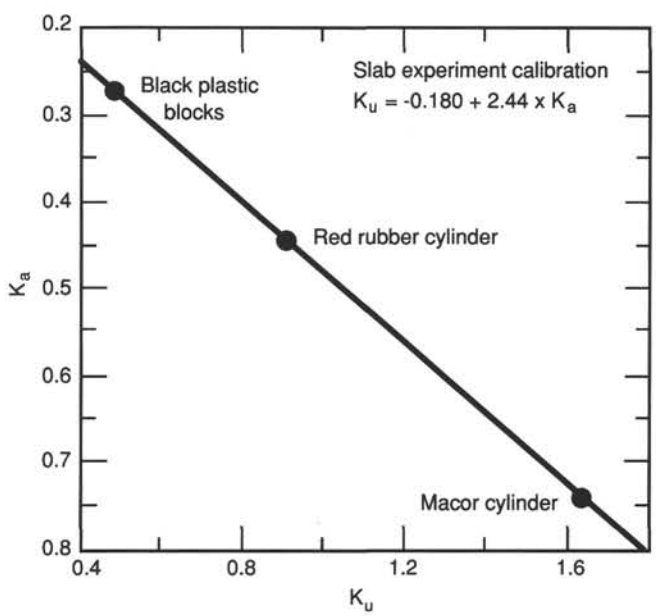

Figure 10. Comparison of conductivity of three reference materials measured by the needle probe and the half-space methods. The temperature histories for both experiments were reduced using equation (2) (see "Physical Properties" section, this chapter).

quate signal strength. Velocities were calculated from the determination of the traveltime of a 500-kHz compressional wave through a measured thickness of sample using a Hamilton Frame Velocimeter and Tektronix DC 5010 counter/timer system. Samples of soft sediment were taken with a special parallel-sided sampling tool. A double-bladed diamond saw was used to obtain samples from more lithified sediments. Basement rock samples were obtained using either a double-bladed diamond saw or a 2.5-cm diameter rock corer. Sample thicknesses (distance) were measured directly from the frame lead screw.

Zero travel times for the velocity transducers were estimated by linear regression of the traveltime vs. distance for a series of aluminum and lucite standards. Filtered seawater was used to improve the acoustic contact between the sample and the transducers. Velocities were not recorded when insufficient or extremely variable signals were obtained.

Electrical Resistivity and Formation Factor

The electrical resistivity of the sediments was measured every 30 cm using a four-electrode (Wenner) configuration. The electrodes are made of 2-mm diameter stainless steel rods with an electrode spacing of 13 mm. A 20-kHz square wave current is applied on the outer electrodes and the difference in potential between the two inner electrodes is measured. The size of the current (typically 50 ma) is measured over a resistor in the outer circuit. For an infinite and homogeneous medium, the resistivity in ohm-m is given by Equation (5) (Jakosky, 1940):

$$\rho = K \cdot \Delta V/I \tag{5}$$

where ρ is the specific resistivity, K is the cell constant, ΔV is the potential difference between the inner electrodes, and I is the current. The primary objective of measuring the resistivity is to determine the formation factor:

$$F = \rho/\rho_W \tag{6}$$

where ρ_W is the resistivity of the pore fluid. We assume that the pore fluid is not substantially different from seawater of normal 3.5% salinity. The resistivity of a seawater standard held in a core liner was measured at the start and end of each core. The formation factor is then computed as the resistivity of the sediment relative to the seawater standard. The uncertainty introduced by making the assumption that the pore-water resistivity is the same as for a seawater standard solution is small.

The formation factor was measured in both the horizontal (across the core) and vertical (along the core axis) directions. Edwards et al. (1984) note that bedding in sediments can give rise to anisotropic eletrical properties. In addition to the mean formation factor,

$$F = F_H F_V, \tag{7}$$

where F_H is the horizontal formation factor, and F_V is the vertical formation factor, we may define the degree of anisotropy, f. Then

$$f = F_V/F_H, \tag{8}$$

f is approximately 1 in isotropic media, but can be high in bedded shales where the grain shape contributes to the anisotropy. The degree of anisotropy is, in part, an expression of the degree to which grains and minerals are aligned parallel to the bedding.

Index Properties

Index properties, wet- and dry-bulk density, grain density, porosity, water content, water ratio and void ratio were determined on samples of sediment and rock (Shipboard Scientific Party, 1988b). Where possible, samples for index property analyses were taken once per section adjacent to compressional-wave velocity and/or electrical resistivity measurements. Samples were weighed using two calibrated Scientech 202 electronic balances. Samples were vacuum dried for at least 12 hr. Dry volumes were measured using a Quantochrome Helium Penta-Pycnometer. Wet volumes were calculated from the dry volumes and the weights as:

$$\text{Wet Volume} = \text{Dry Volume} + (\text{Wet Weight} - \text{Dry Weight})/(0.965 \cdot 1.0245)$$

where 0.965 is the salt factor to correct for the salt precipitated from the pore water, assumed to be standard seawater of 3.5% salinity, and 1.0245 is the density of standard seawater at room temperature.

Porosities and water contents are reported as percent; water contents are on a wet weight basis so that both porosity and water content are a measure of the fraction of water in the total sample. In addition, the water ratios (more commonly called dry water content) and the void ratios were calculated. Wet and dry bulk densities, and grain densities are recorded in gm/cm^3. All values are corrected for salt content of the pore fluid, assuming seawater salinity of 3.5%.

DOWNHOLE MEASUREMENTS

General

Downhole measurements determine the physical and chemical properties of formations adjacent to the borehole. Interpretation of these continuous, *in situ* measurements can yield a stratigraphic, lithologic, structural, geophysical, and geochemical characterization of the subsurface section at the site. After coring is completed, a combination of sensors are lowered downhole on a seven-conductor cable, and each of several measuring devices continuously monitors properties of the adjacent formation. Of the dozens of different combinations commonly used in the petroleum industry, three combinations of Schlumberger sensors were used on Leg 127: (1) the geophysical/lithodensity combination, (2) the geochemical combination, and (3) the formation microscanner (FMS). Specialty tools including the borehole televiewer (BHTV), the Lamont-Doherty temperature tool, and the Barnes/Uyeda water sampler and temperature probe were also run. Each combination or tool was not necessarily deployed in each hole drilled; reference should be made to individual site chapters for details. A packer run was attempted at one site but abandoned before inflation because of hole conditions.

The geophysical logging combination used on Leg 127 consists of the dual induction tool (DIT), the sonic tool (LSS), the lithodensity tool (HLDT), and the L-DGO temperature tool (TLT). This tool combination measures electrical resistivity, compressional-wave velocity, formation density, the spectral content of naturally-occurring radiation, and temperature. The geochemical combination consists of a natural gamma-ray spectrometry tool (NGT), an aluminum clay tool (ACT), an induced gamma-ray spectrometry tool (GST), and the L-DGO temperature tool (TLT). Relative silicon, calcium, iron, sulfur, manganese, hydrogen, chlorine, potassium, thorium, and uranium concentrations were derived from these measurements.

The formation microscanner is a microresistivity imaging device that was deployed for only the second time in the Ocean Drilling Program during Leg 127. It allows for the visual characterization of the borehole wall from measurements related to the electrical resistivity of the formation at the borehole wall.

The borehole televiewer (BHTV) was run following completion of drilling into basement at Site 794 before and after the

straddle packer test, and at Site 795. The BHTV was deployed to image any induced or natural fractures or breakouts and their azimuthal orientation.

The Barnes/Uyeda water sampler (Yokota et al., 1979) and temperature probe (WSTP) allows temperature measurements to be made and pore waters to be sampled in sediments ahead of the drill bit as drilling through unconsolidated and semiconsolidated sediments proceeds. Temperature measurements are used to determine the vertical temperature gradients in the sediments and are used together with measurements of thermal conductivity to determine heat flow through the seafloor (Hyndman et al., 1987) Pore-water samples are analyzed for various chemical species and provide information on the pore-water flow through sediments, and on the chemical exchange between oceanic crust and ocean waters (Geiskes, 1974). A vigorous program of bottom-hole temperature measurements was done for all of the holes on Leg 127. The temperature probe was used every third core to measure temperature in APC- or XCB-drilled holes, providing a value every 30 m if all measurements were successful. The water sampler was used less frequently.

Measurement Devices

A brief description of *in-situ* sensors and measurement devices run during Leg 127 is given below. A more detailed description of the physical principles of these sensors and their applications is provided in Schlumberger (1972), Ellis (1987) and other references cited below.

Electrical Resistivity

The dual induction instrument (DIT) provides three different measurements of electrical resistivity, each with a different radial depth of investigation. Two induction devices ("deep" and "medium" resistivity) send high- frequency alternating currents through transmitter coils, creating magnetic fields that induce secondary (Foucault) currents in the formation. These ground-loop currents produce new inductive signals, proportional to the conductivity of the formation, which are recorded by a series of receiving coils. The measured conductivities are converted to resistivities. A third device (the "spherically" focused resistivity, SFR), measures the current necessary to maintain a constant voltage-drop across a fixed interval. The vertical resolution is of the order of 2 m for the two induction devices, and about 1 m for the spherically focused resistivity device.

To a first order, resistivity responds to the inverse square root of porosity (Archie, 1942). In addition, water salinity, clay content, hydrocarbon content, and temperature are important factors controlling the electrical resistivity of rocks. Other factors that may influence the resistivity of a rock include the concentration of hydrous and metallic minerals, the presence of vesicles, and the geometry of intercorrected pore space.

Sonic Velocity

The digital sonic measurement (Long Spaced Sonic—LSS) uses two acoustic transmitters and two receivers to measure the time required for sound waves to travel along the borehole wall over source-receiver distances of 2.4, 3.0, and 3.6 m (8, 10, and 12 ft). The raw data are expressed as time (microseconds) required for a sound wave to travel through 0.31 m (1 ft) of formation; these traveltimes are then converted to sonic velocities. First arrivals for the individual source-receiver paths are used to calculate the velocities of the different waves traveling in the formation (e.g., compressional, shear, etc.). Only compressional-wave velocity is determined aboard the ship, but the full sonic waveforms are recorded for post-cruise processing to determine shear- wave and Stoneley wave velocities. The vertical resolution of the tool is 0.61 m (2 ft). Compressional-wave velocity is dominantly controlled by porosity and lithification; decreases in porosity and increases in lithification generally cause velocity to increase with depth.

Temperature

The L-DGO temperature tool is a self-contained tool that can be attached to any of the sensor combinations. Data from two thermistors and a pressure transducer are collected every 0.5 to 5.0 s and stored within the tool. Once the *in-situ* measurement is completed the data are transferred to a shipboard computer for analysis. The fast-response thermistor, though low in accuracy, is able to detect small abrupt temperature excursions caused by fluid flow from the formation. The slow-response thermistor has a high accuracy and can be used to estimate the temperature gradient. Data are recorded as a function of time, with conversion to depth based on the pressure transducer (or preferably, on simultaneous recording by Schlumberger of both depth and time).

Lithodensity Measurement

The lithodensity tool (HLDT) uses a ^{137}Ce gamma-ray source to measure the resulting flux at fixed distances from the source. Under normal operating conditions, the attenuation of gamma rays is caused chiefly by Compton scattering (Ellis, 1987). Formation density is extrapolated from this energy flux by assuming that the atomic weight of most rock-forming elements is approximately twice their atomic number. A photoelectric effect (PE) index is also provided. Photoelectric absorption occurs in the energy window below 150 kev and depends on the energy of the incident gamma ray, the atomic cross section, and the nature of the atom. This measurement is almost independent of porosity and can therefore be used directly as a matrix lithology indicator. The radioactive source and detector array are placed in a tool that is pressed against the borehole wail by a spring-loaded caliper arm. Excessive roughness of the borehole wall allows drilling fluid between the skid and the formation. Consequently, the density measurement will give rise to false low values being recorded. Approximate corrections can be applied using caliper data. The vertical resolution of the measurement is about 0.30 m.

Gamma-ray Spectrometry Measurement

This induced gamma-ray device (GST) consists of a pulsed source of 14 Mev neutrons and a gamma-ray scintillation detector. A surface computer performs spectral analysis of gamma-ray counts resulting from the interactions of neutrons emitted by the source, with atomic nuclei in the formation. Characteristic sets of gamma rays from six elements dominate the spectrum: Ca, Si, Fe, Cl, H, S. As their sum is always unity, they do not reflect the actual elemental composition. Consequently, ratios of these elements are used in interpreting the lithology and porosity of the formation and the salinity of the formation fluid.

Aluminum Clay Measurement

Aluminum abundance as measured by the aluminum clay tool (ACT) is determined by neutron-induced (californium chemical source) gamma-ray spectrometry. The contribution to the gamma-ray spectrum by natural radiation is removed by placing Nal gamma-ray detectors both above and below the neutron source; that above measures the natural radiation before activation and that below, the induced radiation after activation. It is then possible to subtract the naturally-occurring component from the total measured after activation. Calibration to elemental weight percent is performed by taking irradiated core samples, of known volume and density, and measuring their gamma-ray output while placed in a jig attached to the logging tool.

Natural Gamma-Ray Measurement

The natural gamma-ray measurement (NGT) measures the natural radioactivity of the formation. Most gamma rays are emitted by the radioactive isotope ^{40}K, and by the radioactive elements of the uranium and thorium series. The gamma radiation originating in the formation close to the borehole wall is measured by a scintillation detector mounted inside the sonde. The analysis is achieved by subdividing the entire incident gamma-ray spectrum into five discrete energy windows. The total counts recorded in each window, for a specified depth in the well, are processed at the surface to give elemental abundances of potassium, uranium, and thorium.

Radioactive elements tend to be most abundant in clay minerals, and consequently the gamma-ray curve is commonly used to estimate the clay or shale content. There are rock matrices, however, for which the radioactivity ranges from moderate to extremely high values as a result of the presence of volcanic ash, potassic feldspar, or other radioactive minerals.

Borehole Inclination Measurement

The general purpose inclination tool (GAIT) contains a three-component accelerometer and a three-component magnetometer. The device is used to measure the orientation of the downhole sensors within the borehole, the orientation (or deviation) of the borehole itself, and to compensate for instrument accelerations in the axis of the borehole during data acquisition. It is included as a part of the formation microscanner.

Formation Microscanner

The formation microscanner produces high-resolution borehole images from electrical conductivity measurements (Ekstrom et al., 1986; Pezard and Luthi, 1988). Its application as used in the petroleum oil industry since 1986 has been precluded in the Ocean Drilling Program because of constraints imposed by the internal diameter (4.125 in.) of the drill pipe. A modified sensor was consequently developed by Schlumberger for ODP and first deployed during Leg 126. The FMS has a vertical resolution of approximately 1 cm, but a detection threshold for conductive features of the order of micrometers. This fine-scale detection ability (raw data points are recalled every 2.5 mm) allows for the detailed study of subsurface structures. In contrast, typical conventional downhole measurements are averaged over 150 mm; thus the sampling rate of the FMS is consequently 60 times larger than most other logging devices. The FMS has four onhogonal pads that are pressed against the borehole wall. In the original version developed by Schlumberger, two adjacent pads each carry an array of 27 closely-spaced electrodes, from which two electrical images are derived. The electrode currents probe the conductivity of the rock to a depth of a few centimeters into the borehole wall, thus responding to variations in physical and chemical properties of the rock such as porosity or surface conduction. The series of conductivity traces are displayed side-by-side, and coded into an image where black represents the most conductive values and white the most resistive ones. The new ODP sensor was designed in such a way that four images of sixteen traces each are recorded simultaneously instead of two images. In addition, the resolution of the images is improved due to the smaller size of the electrode array. Once the data have been acquired in the borehole, the images are processed on a dedicated workstation to allow for on-site comparison with the cores. In the future, a graphic workstation will be installed on the ship to perform such basic analyses as the interactive mapping of geological features.

Possible applications of the FMS-derived images include: the orientation of cores, the mapping of fractures, foliations, and sedimentary features; and the direct analysis of depositional environments (with information on transport direction, structure of the pore space, nature of contacts, and depositional sequences).

Borehole Televiewer

The borehole televiewer (BHTV) is an acoustic device that scans the wall of a borehole, producing an image of the reflectivity of the rock surrounding the well bore as a function of depth and azimuth. The scientific results obtained from the BHTV logs include the location and orientation of fractures intersecting the well bore, the determination of structural features, the measurement of borehole diameter, surface roughness and ellipticity, and the determination of the principal horizontal stresses from observing the azimuth of breakouts and induced fractures observed in the time-domain images.

Data Management

Downhole data quality may be seriously degraded where the borehole diameter is excessively large or rapidly changing. The nuclear measurements (i.e., density, neutron porosity, and both natural and induced spectral gamma rays) are most seriously impaired because of the large attenuation by the borehole fluid. Electrical resistivity and velocity measurements are least sensitive to such borehole irregularities. Corrections can be applied to the original data to reduce the effects of these conditions.

In addition to borehole rugosity, different logs may have small depth mismatches, caused by either cable stretch or by ship heave during recording. Small errors in depth matching can impare the results in zones of rapidly varying lithology. To minimize such errors, a hydraulic heave compensator adjusts for ship motion in real time. Precise depth matching of downhole data with core data is not obtainable in zones where core recovery is low. This is because of the inherent ambiguity in placing the impartially recovered core within the interval.

Data Analysis

Throughout downhole logging measurements acquisition, incoming data were observed in real time on a monitor oscilloscope and simultaneously recalled on digital tape. After the completion of a set of downhole measurements, tapes were reformatted to allow interpretation using shipboard software; an interactive log-interpretation software package with a versatile array of manipulative and plotting options was used for this purpose. The precise nature of the interpretation procedure varies for each site. Initial appraisal of the downhole data was carried out on board ship, while further analysis and interpretation are undertaken after the end of the leg.

Reprocessing of Downhole Logging Data

Raw count rates for six elements (Ca, Si, Fe, S, Cl, and H) are obtained in real time by the Schlumberger data acquisition software. These count rates have commonly exhibited some interference of chlorine with other elemental count rates during previous ODP legs; this is manifested as a strong but spurious correlation between chlorine and calcium and weaker correlations with other elements measured by the tool. This interference, attributable to the dominance of the induced gamma-ray spectrum by chlorine, has until now been unavoidable in ODP holes because the minimum pipe diameter is too small to permit theuse of a boron sleeve for chlorine count suppression (see Harvey and Lovell, in press). On Leg 126, however, a modification to the tool allowed the inclusion of a slimmer, but perhaps equally efficient boron sleeve.

The compositional data were reprocessed after the cruise using proprietary Schlumberger software. The gamma-ray spectrum at each depth is calculated for titanium, gadolinium, and potassium in addition to the six elements listed above. Although gadolinium is present in concentrations of only a few parts per

million, its neutron capture cross section is so large that gadolinium can account for 10–30% of the total gamma-ray spectrum. Inclusion of these additional elements improves the quality of the overall determination, particularly improving the accuracy of calculated calcium abundance, by converting sources of unaccounted variance to signals. The determined potassium concentrations, however, are less accurate than those from the natural gamma-ray measurement (NGT), and the hydrogen concentrations are similarly less accurate than those from the neutron tool (CNT).

Aluminum concentrations from the ACT require correction for variations in cable speed, which affect the time lag between the neutron irradiation of the formation and the recording of the induced gamma-ray spectrum, because the number of induced gamma rays decreases rapidly with time. Post-cruise correction for this effect is possible using techniques proven in land holes. This correction may be less reliable in ODP holes where ship heave still affects the measurement in spite of mechanical compensation devices.

Upon completion of both the geophysical and geochemical downhole measurement combinations, it is possible for one to carry out further reprocessing of the geochemical downhole data. The relative abundances of Ca, Si, Fe, T, Al, K, S, Th, U, and Gd are used to calculate a log of predicted photoelectric effect. The difference between this calculated curve and the actual photoelectric curve may be attributed to the two major elements not directly measured, Mg and Na. Major elements are converted from volume percent to weight percent using downhole data curves of total porosity (bounds water plus pore water) and density. Major elements are expressed in terms of oxide weight percent, based on the assumption that oxygen is 50% of the total dry weight.

If GST data are available and not enough log typ es are run to permit a complete calculation for the oxide weight percentages, one further processing step is made. Omitting chlorine and hydrogen, the yields of the other GST- derived elements (Ca, Si, Fe, T, S, K and Gd) are summed, and each is expressed as a fraction of this total yield. This procedure corrects for porosity and count-rate variations. Although the absolute abundance of each element is not determined, estimates of downhole variations in relative abundance are produced.

Downhole sonic data obtained in real time are not based on full waveform analyses but on a threshold-measuring technique that attempts to detect the compressional-wave arrival from the first waveform eclipsing a noise threshold at each offset. Occasionally this technique fails and either the threshold is exceeded by noise or the amplitude of the first compressional arrival is smaller than the threshold. The latter of these effects is known as cycle skipping and creates spurious spikes on the sonic log. Such problems may often be eliminated by reprocessing the data.

Synthetic Seismogram

The velocity structure determined from the edited sonic log was used to construct a synthetic seismogram. A synthetic seismogram provides a good way of correlating downhole velocity measurements with the surface refraction and reflection profiles. Evaluation of the synthetic seismogram also helps in the interpretation of the vertical seismic profile.

In-Situ Stress Measurements using the FMS

The formation microscanner was used during Leg 127 to determine principal horizontal stress directions from elongation due to stress-induced borehole breakouts. In an isotropic, linearly elastic rock subject to differential stresses, breakouts form along the borehole wall as a result of compressive stress concentrations exceeding the strength of the rock. Under these conditions, the breakout orientation will develop in the direction of the least principal horizontal stress. It has been demonstrated in different areas that stress orientations deduced from breakouts are consistent with other independent indicators (Bell and Gough, 1979; Zoback et al., 1988).

REFERENCES

Akiba, F., 1985. Middle Miocene to Quaternary diatom biostratigraphy in the Nankai Trough and Japan Trench, and modified lower Miocene through Quaternary diatom zones for middle-to-high latitudes of the North pacific. *In* Kagami, H., Karig, D. E., et al., *Init. Repts. DSDP*, 87: Washington (U.S. Govt. Printing Office), 393–482.

Akiba, F., and Yanagisawa, Y., 1985. Taxonomy, morphology and phylogeny of the Neogene diatom zonal marker species in the middle-to-high latitudes of the North Pacific. *In* Kagami, H., Karig, D. E., et al., *Init. Repts. DSDP*, 87: Washington (U.S. Govt. Printing Office), 483–554.

Archie, G. E., 1942. The electrical resistivity log as an aid in determining some reservoir characteristics. *J. Pet. Tech.*, 5:1–8.

Asano, K., Ingle, J. C., Jr., and Takayanagi, Y., 1969. Neogene planktonic foraminiferal sequence in northern Honshu. *In* Bronniman, R. P., and Renz, H. (Eds.), *Proc. 1st Int. Conf. Planktonic Microfossils*, Leiden (E. J. Brill), 1:14–25.

Bell, J. S., and Gough, D. I., 1979. Northeast-Southwest compressive stress in Alberta: evidence from oil wells. *Earth Planet. Sci. Lett.*, 45:475–482.

Berggren , W. A., Kent, D. V., Flynn, J. J., and Van Couvering, J. A., 1985a. Cenozoic geochronology. *Geol. Soc. Am. Bull.*, 96:1407–1418.

Berggren, W. A., Kent, D. V., and Van Couvering, J. A., 1985b. The Neogene: Part 2. Neogene geochronology and chronostratigraphy. *In* Snelling, N. J. (Ed.), *The Chronology of the Geological Record*: Geol. Soc. London Mem., 10:211–260.

Blow, W. H., 1969. Late middle Eocene to Recent planktonic foraminiferal biostratigraphy. *In* Bronniman, R. P., and Renz, H. H. (Eds.), *Proc. 1st Int. Conf. Planktonic Microfossils*: Leiden (E. J. Brill), 1: 199–421.

Boyce, R. E., 1976. Definitions and laboratory techniques of compressional sound velocity parameters and wet- water content, wet-bulk density, and porosity parameters by gravimetric and gamma ray attenuation techniques. *In* Schlanger, S. O., Jackson, E. D., et al., *Init. Repts. DSDP*, 33: Washington (U.S. Govt. Printing Office), 931- 958.

Bukry, D., 1978. Biostratigraphy of Cenozoic marine sediment by calcareous nannofossils. *Micropaleontology*, 24:44–60.

Burckle, L. H., 1977. Pliocene and Pleistocene diatom datum levels from the equatorial Pacific. *Quat. Res.*, 7:330–340.

Burckle, L. H., Keigwin, L. D., and Opdyke, N. D., 1982. Middle and late Miocene stable isotope stratigraphy: correlation to the paleomagnetic reversal record. *Micropaleontology*, 28:329–334.

Burckle, L. H., and Trainer, J., 1979. Middle and late Pliocene diatom datum levels from the central Pacific. *Micropaleontology*, 25:281–293.

Craig, R. F., 1983. *Soil Mechanics*: Wokingham, Berkshire, U.K. (Van Nostrand Reinhold).

Dunham, R. J., 1962. Classification of carbonate rocks according to depositional texture. *In* Ham, W. E. (Ed.), *Classification of Carbonate Rocks*: AAPG Mem., 1: 108–121.

Edwards, R. N, Nobes, D. C., and Gomez-Treviño, E., 1984. The effects of interbedding in a sedimentary basin. *Geophysics*, 49: 544–549.

Ekstrom, M. P., Dahan, C. A., Chen, M.-Y., Lloyd, P. M., and Rossi, D. J., 1986. Formation imaging with microelectrical scanning arrays. Trans. *SPWLA 27th Ann. Logging Symp.*, Paper BB.

Ellis, D. V., 1987. *Well Logging for Earth Scientists*: Amsterdam (Elsevier).

Embry, A. F., and Kloven, E. J., 1972. Absolute water depth limits of late Devonian paleoecological zones. *Geol. Resch.*, 61:672–686.

Emeis, K.-C. and Kvenvolden, K. A., 1986. Shipboard organic geochemistry on *JOIDES Resolution*. *ODP Tech. Note*, 7: College Station, TX (Ocean Drilling Program).

Fisher, R. V., and Schmincke, H.-U., 1984. *Pyroclastic rocks*: New York (Springer-Verlag).

Foreman, H. P., 1975. Radiolaria from the North Pacific, Deep Sea Drilling Project, Leg 32. *In* Larson, R. L., Moberly, R., et al., *Init. Repts. DSDP*, 32: Washington (U.S. Govt. Printing Office), 579–676.

Gealy, E. L., Winterer, E. L., and Moberly, R., Jr., 1971. Methods, conventions, and general observations. *In* Winterer, E. L., Reidel, W. R., et al., *Init. Repts. DSDP*, 7 (Pt. 1): Washington (U.S. Govt. Printing Office), 9–26.

Gieskes, J. M., 1974. Interstitial water studies, Leg 25. *In* Simpson, E.S.W, Schlich, R., et al., *Init. Repts. DSDP*, 25: Washington (U.S. Govt. Printing Office), 361–394.

Gieskes, J. M., and Peretsman, G., 1986. Water chemistry procedures aboard JOIDES Resolution—some comments. *ODP Tech. Note*, 5: College Station, TX (Ocean Drilling Program).

Harvey, P. K., and Lovell, M. A., in press. Basaltic lithostratigraphy of DSDP Hole 504B. *Nuclear Geophysics*.

Hearst, J. R., and Nelson, P. H., 1985. *Well Logging for Physical Properties*: New York (McGraw Hill).

Hodell, D. A., and Kennett, J. P., 1986. Late Miocene-early Pliocene stratigraphy and paleoceanography of the South Atlantic and southwest Pacific Oceans: a synthesis. *Paleoceanography*, 1:285–311.

Hyndman, R. D, Langseth, M. G., and Von Herzen, R. P., 1987. Deep Sea Drilling Project geothermal measurements: a review. *Rev. Geophys.*, 25:1563–1582.

Ingle, J. C., 1973. Neogene foraminifera from the north eastern Pacific Ocean, Leg 18. *In* Kulm, L. D., von Huene, R., et al., *Init. Repts. DSDP*, 18: Washington (U.S. Govt. Printing Office), 517–568.

Jakosky, J. J., 1940. *Exploration Geophysics*: Los Angeles (Times-Mirror Press).

Jenkins, D. G., and Srinivasan, M. S., 1986. Cenozoic planktonic foraminifers from the equator to the sub- antarctic of the southwest Pacific. *In* Kennett, J. P., von der Borch, C., et al., *Init. Repts. DSDP*, 90 (Pt. 2): Washington (U.S. Govt. Printing Office), 795–834.

Johnson, D. A., and Nigrini, C. A., 1985. Synchronous and time-transgressive Neogene radiolarian events in the tropical Indian and Pacific Oceans. *Mar. Micropaleontol.*, 9:489–523.

Katz, B. J., 1983. Limitations of Rock-Eval pyrolysis for typing organic matter. *Org. Geochem.*, 4:195–199.

Keller, G., Barron, J. A., and Burckle, L. H., 1982. North Pacific Late Miocene correlations using microfossils, stable isotopes, percent $CaCO_3$, and magnetostratigraphy. *Mar. Micropaleontol.*, 7:327–357.

Kennett, J. P., and Srinivasan, M. S., 1983. *Neogene Planktonic Foraminifera: a Phylogenetic Atlas*: Stroudsburg, PA (Hutchinson Ross).

Koizumi, I., 1985. Diatom biochronology for late Cenozoic northwest Pacific. *J. Geol. Soc. Japan*, 91:195–211.

Koizumi, I., and Tanimura, Y., 1985. Neogene diatom biostratigraphy of the middle latitude western North Pacific, Deep Sea Drilling Project Leg 86. *In* Heath, G. R., Burckle, L. H., et al., *Init. Repts. DSDP*, 86: Washington (U.S. Govt. Printing Office), 269–300.

Lagoe, M. B., and Thompson, P. R., 1988. Chronostratigraphic significance of late Cenozoic planktonic foraminifera from the Ventura Basin, California: potential for improving tectonic and depositional interpretation. *J. Foram. Res.*, 18:250–266.

Ling, H.Y., 1975. Radiolaria: Leg 31 of the Deep Sea Drilling Project. *In* Karig, D. E., Ingle, J. C. Jr., et al., *Init. Repts. DSDP*, 31: Washington (U.S. Govt. Printing Office), 703–761.

Maiya, S., Saito, T., and Sato, T., 1976. Late Cenozoic planktonic foraminiferal biostratigraphy of northwest Pacific sedimentary sequences. *In* Takayanagi, U., and Saito, T. (Eds.), *Progress in Micropaleontology*: New York (Micropaleontology Press), 395–422.

Manheim, F. T., and Sayles, F. L., 1974. Composition and origin of interstitial waters of marine sediments based on deep sea drill cores. *In* Goldberg, E. D. (Ed.), *The Sea* (Vol. 5): New York (Wiley-Interscience), 527–568.

Matoba, Y., 1984. Paleoenvironment of the Sea of Japan. *In* Oertli, H. J. (Ed.), *Benthos '83, 2nd Int. Symp. Benthic Foraminifera* (Pau, April 1983), 409–414.

Mazzulo, J., and Graham, A. G., 1988. Handbook for Shipboard Sedimentologists, *ODP Technical Note 8*: College Station, TX (Ocean Drilling Program).

Nakaseko, K., and Sugano, K., 1973. Neogene radiolarian zonation in Japan. *Geol. Soc. Japan Mem.*, 8:23.

Natland, J. H., 1978. Crystal morphologies in basalt from DSDP Site 395, 23°N, 46°W, mid-Atlanic Ridge. *In* Melson, W. G., Rabinowitz, P. D., et al., *Init. Repts. DSDP*, 45: Washington (U.S. Govt. Printing Office), 423– 445.

Natland, J. H., 1980. Crystal morphologies in basalts dredged and drilled from the east Pacific rise near 9°N and the Siqueiros fracture zone. In Rosendahl, B. R., Hekinian, R., et al., *Init. Repts. DSDP*, 54: Washington (U.S. Government Printing Office), 605–634.

Norrish, K., and Hutton, J. T., 1969. An accurate X-ray spectrographic method for the analysis of a wide range of geological samples. *Geochim. Cosmochim. Acta*, 33:431–453.

Oda, M., 1986. Some aspects and problems concerned with microfossil biochronology for the Neogene in central and northeast Honshu, Japan. *In* Nakagawa, H., Kotaka, T., and Takayanagi, Y. (Eds.), *The Essays on Geology of Professor N. Kitamura*: Sendai (Sasaki Print Co.), 195–211.

Perch-Nielsen, K., 1985. Cenozoic calcareous nannofossils. In Bolli, H. M., Saunders, J. B., and Perch-Nielsen, K. (Eds.), *Plankton Stratigraphy*: Cambridge (Cambridge University Press), 427–554.

Peters, K. E., 1986. Guidelines for evaluating petroleum source rock using programmed pyrolysis. *AAPG Bull.*, 70:318–329.

Pezard, P. A., and Luthi, S. M., 1988. Borehole electrical images in the basement of the Cajon Pass Scientific Drillhole, California; fracture identification and tectonic implications. *Geophys. Res. Lett.*, 15: 1017–1020.

Rahman, A., and Roth, P. H., 1989. Late Neogene calcareous nannofossil biostratigraphy of the Gulf of Aden region based on calcareous nannofossils. *Mar. Micropaleont.*, 15:1–27.

Reynolds, R. A., 1980. Radiolarians from the western North Pacific, Leg 57, Deep Sea Drilling Project. *In* Scientific Party, *Init. Repts. DSDP*, 56, 57 (Pt. 2): Washington (U.S. Govt. Printing Office), 735–769.

Reynolds, R. C., 1967. Estimations of mass absorption coefficients by Compton scattering: improvements and extensions of the method. *Am. Mineral.*, 49:1133–1143.

Robinson, P. T., von Herzen, R., et al., 1989. *Proc. ODP, Init. Repts.*, 118: College Station, TX (Ocean Drilling Program).

Roth, P. H., 1974. Calcareous nannofossils from the northwestern Indian Ocean, Leg 24, Deep Sea Drilling Project. *In* Fisher, R. L., Bunce, E. T., et al., *Init. Repts. DSDP*, 24: Washington (U.S. Govt. Printing Office), 969–994.

Saito, T., 1963. Miocene planktonic foraminifera from Honshu, Japan. *Tohoko Univ. Sci. Rep. 2nd Ser.* (Geol.), 35(2):123–209.

Sanfilippo, A., Westberg-Smith, M. J., and Riedel, W. R., 1985. Cenozoic Radiolaria. In Bolli, H. M., Saunders, J. B., and Perch-Nielsen, K. (Eds.), *Plankton Stratigraphy*: Cambridge (Cambridge University Press), 631–712.

Schlumberger, Ltd., 1972. *Log Interpretation* (Vol. 1, Principles): New York (Schlumberger, Ltd.).

Shepard, F. P., 1954. Nomenclature based on sand-silt-clay ratios. *J. Sediment. Petrol.*, 24:151–158.

Shipboard Scientific Party, 1988a. Explanatory Notes: Leg 112. *In* Suess, E., von Huene, R., et al., *Proc. ODP, Init. Repts.*, 112: College Station, TX (Ocean Drilling Program), 25–44.

Shipboard Scientific Party, 1988b. Explanatory notes. *In* Ciesielski, P. F., Kristoffersin, Y., et al., *Proc. ODP, Init. Repts.*, 114: College Station, TX (Ocean Drilling Program), 3–22.

Vacquier, V., 1985. The measurement of thermal conductivity of solids with a transient linear heat source on the plane surface of a poorly conducting body. *Earth Planet Sci. Lett.*, 74:275–279.

von Herzen, R. P., and Maxwell, A. E., 1959. The measurements of thermal conductivity of deep-sea sediments by a needle probe method. *J. Geophys. Res.*, 64: 1557–1563.

Wentworth, C. K., 1922. A scale of grade and class terms for clastic sediments. *J. Geol.*, 30:377–392.

Yokota, I., Kinoshita, K., and Uyeda, S., 1979. New DSDP (Deep Sea Drilling Project) downhole temperature probe utilizing digital self-recording system with IC RAM elements. *Bull. Earthquake Res. Inst. Univ. Tokyo*, 54:441–462.

Zoback, M. D., Zoback, M. L., Mount, V. S., Suppe, J., Eaton, J. P., Healy, J. H., Oppenheimer, D., Reasenberg, P., Jones, L., Raleigh, C. B., Wong, I. G., Scotti, O., and Wentworth, C., 1988. New evidence on the state of stress of the San Andreas Fault. *Science*, 238: 1105–1111.

Ms 127A-102